HHT-α and TR-BDF2 schemes for dynamic contact problems

Hao Huang, Nicolas Pignet, Guillaume Drouet, Franz Chouly

HHT-α and TR-BDF2 schemes for dynamic contact problems

Hao Huang[1,2], Nicolas Pignet[1], Guillaume Drouet[1], and Franz Chouly[2,3,4]

[1]EDF Lab Paris-Saclay, 7 boulevard Gaspard Monge, 91120 Palaiseau, France
[2]Institut de Mathématiques de Bourgogne, Université de Bourgogne Franche-Comté, 21078 Dijon, France
[3]Center for Mathematical Modeling and Department of Mathematical Engineering, University of Chile and IRL 2807 - CNRS, Santiago, Chile
[4]Departamento de Ingeniería Matemática, CI^{2}MA, Universidad de Concepción, Casilla 160-C, Concepción, Chile

March 30, 2023

Abstract

This work focuses on the numerical performance of HHT-α and TR-BDF2 schemes for dynamic frictionless unilateral contact problems between an elastic body and a rigid obstacle. Nitsche's method, the penalty method, and the augmented Lagrangian method are considered to handle unilateral contact conditions. Analysis of the convergence of an opposed value of the parameter $\tilde{\alpha}$ for the HHT-α method is achieved. The mass redistribution method has also been tested and compared with the standard mass matrix. Numerical results for 1D and 3D benchmarks show the functionality of the combinations of schemes and methods used.

Key words: contact problem, Nitsche's method, augmented Lagrangian method, finite elements, elastodynamics, time-marching schemes.

1 Introduction

One of the main tools for numerical simulation for solid mechanic problems is the finite element method. In the industry, contact problems are omnipresent, and many traditional methods cannot provide acceptable solutions in the context of elastodynamics: they are too influenced by parasitic oscillations or do not conserve energy. A difficulty is that this type of problem has a nonlinear boundary condition on the displacement field. The main existing methods for discretizing the Signorini contact conditions are the method of penalization, mixed/mortar methods, Nitsche's method, or the augmented Lagrangian method. Improvements in the accuracy and numerical robustness of these simulations are always expected by industry and researchers.

Usually, the time-space discretization involves the problems of choosing: (i) the finite element space; (ii) the enforcement of the contact condition, and (iii) the time-stepping scheme.

The idea concerned in this work for treating the nonlinear boundary condition is to transfer the constrained optimization problems to an unconstrained problem or a sequence of unconstrained problems. This approach for contact problems in the static case is largely discussed by Kikuchi and Oden [40, 48, 49]. In the dynamic case, several schemes, *e.g.*, (modified) Crank-Nicolson, Newmark, HHT schemes [2, 27, 38, 43], Paoli-Schatzman schemes [51, 52], or more recently [26], to mention a few, have already been considered and problems of spurious oscillations and numerical instabilities caused by artificial energy creation have been reported [42].

Nitsche's method was originally introduced for the treatment of the Dirichlet boundary conditions as a consistent method without additional Lagrangian multipliers [46]. In recent years, it has been introduced for contact problems. Firstly proposed for frictionless unilateral contact in linear elasticity as the classical symmetric version in [15] and as variants (symmetric, skew-symmetric, and non-symmetric) versions in [21]. Then, the frictional case was considered for Tresca friction in [11, 12, 22] and for Coulomb friction in [44, 58], with several analyses of a posteriori error estimates [14, 31]. An extension to large strain bilateral contact has also been performed in [61]. The works on dynamic contact with Nitsche's method begin from [19, 20]. This method yields a well-posed semi-discrete problem in space (discretization in space by finite element method and continuous in time with the conservation of modified energy for the symmetric variant). Different time-marching schemes can then be applied to discretize in time: the explicit Verlet scheme in [23], for the implicit schemes, the θ-scheme and Newmark scheme in [13, 17, 18], and some IMEX schemes in [6]. A new "hybrid" scheme has also been introduced in [17].

The idea of the augmented Lagrangian method (ALM) originated from Hestenes [33] and Powell [54] independently [53] and was finally established by Fortin, Glowinski, and Le Tallec [29, 30] as a method for problems of minimization with equality constraints. Like Nitsche's method, ALM is also a consistent method. A first implementation of this method for contact problems with Coulomb's friction law was established by Alart and Curnier [1] and in recent years, convergence analysis for several reformulations have been realized by Burman et al. [8]. A review of the static case for both essential and inequality boundary conditions can be found in [9]. In Burman et al. [8], the link between Nitsche and ALM is also emphasized. In fact, the methods are very similar: Nitsche involves fewer unknowns but ALM allows more flexibility to discretize the contact pressure. Few references can be found for applications in the dynamics case via the ALM (and finite element method). We can refer for instance the work of [37].

For structural dynamic problems, methods of time integration for second-order differential equations are required and different time-marching schemes have been largely applied. The HHT-α scheme is a classical and representative method for elastodynamic problems proposed by Hilber, Hughes, and Taylor [34]. This scheme has been proved to be an A-stable method for linear elastodynamic cases and is widely used for solving, *e.g.*, the dynamic of systems of mass points, rigid bodies, or combined with finite element method. In recent years, analysis of the HHT-α method for nonlinear problems was attracting more attention [28], and for contact problems, this method has been tested with other methods such as pure contact or penalty [27, 43]. It can be considered as a general case of the family of Newmark schemes [45], and there exists the generalized-α method as a possible extension [24].

Another main scheme concerned in this work is the TR-BDF2 scheme (also known as the Bathe scheme [4]), which is an implicit scheme with 2 sub-steps: the first sub-step uses the trapezoidal rule and the second sub-step uses a three-point backward difference approximation. This scheme was proposed targeted to the nonlinear dynamic problems where the Crank-Nicolson method and the Wilson-θ method [5] may fail to provide a stable solution. It can also be considered an implicit predictor-corrector scheme.

In this work, we focus on the evolution of the impact of a linear elastic body and a rigid obstacle. We want particularly to study how to combine time-marching schemes as HHT-α and TR-BDF2 schemes with contact via Nitsche's method, and possibly with the mass redistribution method. For instance, these two kinds of schemes have not been applied with Nitsche's method or ALM. We present then some simulation results with 1D and 3D benchmarks using these different methods. By testing their performances, we are particularly interested in the influence of the numerical parameters, the parasitic oscillation associated with the contact surface due to the discontinuity in time, and the conservation or not of the total energy for the time-marching schemes. The new combinations applied in this work can eventually improve upon existing methods by providing better accuracy and numerical robustness for nonlinear (and non-regular) dynamic problems.

This paper is organized as follows. We first introduce the mathematical models treating the Signorini boundary conditions and the semi-discretization of the elastodynamic problem in Sect. 2. In Sect. 3, we present the two time-marching schemes (HHT-α and TR-BDF2 method) as well as some analysis on convergence for an opposed parameter $\tilde{\alpha}$ for HHT-α method. In Sect. 4, we are going to show three benchmarks, including a new 1D benchmark with an analytic solution, with their numerical simulations. Moreover, the mass redistribution method [25] has been applied and compared for the two 1D benchmarks, and the hybrid Nitsche scheme [20] has been tested with the 3D benchmark.

2 Contact problem and choosing of the enforcement of contact condition

We consider an elastic body $\Omega \subset \mathbb{R}^d, d \in \{1, 2, 3\}$, see Fig. 1. On the boundary $\partial\Omega := \Gamma_D \cup \Gamma_N \cup \Gamma_C$ of Ω, Dirichlet, Neumann, and Signorini boundary conditions are applied respectively on the disjoint subsets Γ_D, Γ_N, and Γ_C.

We seek the displacement field $\mathbf{u} : \Omega \times (0, T) \to \mathbb{R}^d$, where $T > 0$ is the final time, verifying the equations (1):

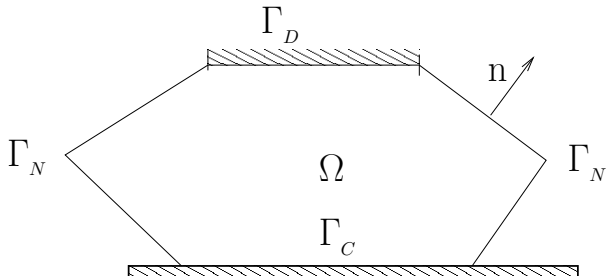

Figure 1: Elastic body occupying the domain Ω, with the boundary $\partial\Omega$.

$$
\begin{aligned}
\rho\ddot{\mathbf{u}} - \operatorname{div}(\sigma(\mathbf{u})) &= \mathbf{f}(t), \ \text{in } \Omega\times(0,T), && \text{(i)}\\
\sigma(\mathbf{u}) &= \lambda\ \operatorname{tr}(\epsilon(\mathbf{u}))\mathbf{I} + 2\mu\epsilon(\mathbf{u}), \ \text{in } \Omega\times(0,T), && \text{(ii)}\\
\mathbf{u} &= \mathbf{0}, \ \text{on } \Gamma_D\times(0,T), && \text{(iii)}\\
\sigma(\mathbf{u})\cdot\mathbf{n} &= \mathbf{f}_N(t), \ \text{on } \Gamma_N\times(0,T), && \text{(iv)}\\
u_n \le 0, \quad \sigma_n(\mathbf{u}) \le 0, \quad u_n\sigma_n(\mathbf{u}) &= 0, \ \text{on } \Gamma_C\times(0,T), && \text{(v)}\\
\sigma(\mathbf{u})\cdot\mathbf{n} - \sigma_n(\mathbf{u})\cdot\mathbf{n} &= \mathbf{0}, \ \text{on } \Gamma_C\times(0,T), && \text{(vi)}\\
\mathbf{u}(\cdot,0) = \mathbf{u}_0, \quad \dot{\mathbf{u}}(\cdot,0) &= \dot{\mathbf{u}}_0, \ \text{in } \Omega. && \text{(vii)}
\end{aligned}
\tag{1}
$$

The equations (i) - (iv) describe the problem of elastodynamics in small deformation, where ρ is the mass density, $\mathbf{f}(t)$ is the volumetric source term, $\mathbf{f}_N(t)$ is the surface charge, λ and μ are Lamé coefficients, $\operatorname{tr}(\cdot)$ denotes the trace of a matrix, $\epsilon(\cdot) := \frac{1}{2}\left(\nabla(\cdot) + \nabla^T(\cdot)\right)$ is the deformation tensor and $\mathbf{I}$ is the identity matrix of dimension d. The equations (v) and (vi) denote Signorini's condition for frictionless contact, where $u_n = \mathbf{u}\cdot\mathbf{n}$, $\sigma_n(\mathbf{u}) = (\sigma(\mathbf{u})\cdot\mathbf{n})\cdot\mathbf{n}$ are respectively the normal displacement and the contact pressure at boundary Γ_C. The initial conditions at the time $t = 0$ on the initial displacement and velocity fields are given in equation (vii). We also introduce the bilinear and linear forms

$$
\begin{aligned}
a(\mathbf{u},\mathbf{v}) &:= (\sigma(\mathbf{u}), \epsilon(\mathbf{v}))_\Omega\,,\\
l(t)(\mathbf{v}) &:= (\mathbf{f}(t),\mathbf{v})_\Omega + (\mathbf{f}_N(t),\mathbf{v})_{\Gamma_N}\,,
\end{aligned}
\tag{2}
$$

where the notation $(\mathbf{u},\mathbf{v})_\Omega := \int_\Omega \mathbf{u}\cdot\mathbf{v}\ \mathrm{d}\Omega$ and $(\mathbf{u},\mathbf{v})_{\Gamma_C} := \int_{\Gamma_C}\mathbf{u}\cdot\mathbf{v}\ \mathrm{d}\Gamma_C$ are the L^2-products defined on Ω and Γ_C respectively. The associated norms are denoted by $||\cdot||_\Omega := (\cdot,\cdot)_\Omega^{\frac{1}{2}}$ and $||\cdot||_{\Gamma_C} := (\cdot,\cdot)_{\Gamma_C}^{\frac{1}{2}}$.

Let $\mathbf{V}^h$ be the Lagrange finite element space to discretize the displacement, of degree one or two ($k = 1$ or 2), and based on a mesh $\mathcal{T}^h$ of the domain Ω:

$$
\mathbf{V}^h := \left\{\mathbf{v}^h \in \left(C^0(\overline{\Omega})\right)^d : \mathbf{v}|_{\Gamma_D} = \mathbf{0};\ \mathbf{v}|_T = \mathbb{P}_k(T),\ \forall T\in\mathcal{T}^h\right\}. \tag{3}
$$

We also introduce the space W^h defined as the piecewise linear space on Γ_C for the continuous

Lagrange multiplier used for the case $k = 2$:

$$W^h := \left\{ \mu^h \in C^0(\overline{\Gamma_C}) : \mu^h|_{T\cap\Gamma_C} \in \mathbb{P}_1(T),\ \forall T \in \mathcal{T}^h \right\}. \tag{4}$$

The total mechanical energy associated with the solution $\mathbf{u}$ of dynamic Signorini problem (1) is:

$$E(t) = \frac{1}{2}\left(\rho\dot{\mathbf{u}}, \dot{\mathbf{u}}\right)_\Omega + \frac{1}{2}a(\mathbf{u}, \mathbf{u}),\ \forall t \in [0, T]. \tag{5}$$

Moreover, with the persistency condition [2, 32, 43] $(\sigma(\mathbf{u}) \cdot \mathbf{n}) \cdot \dot{\mathbf{u}} = 0$ on Γ_C, and when $l(t)$ vanishes, the evolution of energy

$$\frac{\mathrm{d}}{\mathrm{d}t}E(t) = 0$$

and the total mechanical energy is constant on time.

The enforcement of contact conditions is then introduced at the discrete level, with Nitsche's, penalty and ALM formulations.

2.1 Nitsche's method

Initially introduced by Nitsche [46] (see also [59]), the method has been extended by [15, 21] for the unilateral contact problem, then in elastodynamics [18, 19, 20]. We are going to define the space-discrete weak formulation of the Nitsche-FEM method: firstly, we introduce the linear discrete operator

$$P_N : \begin{array}{ccc} \mathbf{V}^h & \to & L^2(\Gamma_C) \\ \mathbf{v}^h & \mapsto & \sigma_n(\mathbf{v}^h) - \gamma_N v_n^h \end{array}, \tag{6}$$

where γ_N is a positive function independent of $\mathbf{v}$, such that

$$\gamma_{N|T\cap\Gamma_C} = \frac{\gamma_0}{h_T}, \tag{7}$$

so for each triangle T intersected with Γ_C, where h_T is the diameter of the triangle T and γ_0 is a positive constant (the Nitsche parameter). The primal discrete problem is as follows:

$$\begin{cases} \text{Seek } \mathbf{u}^h : [0, T] \to \mathbf{V}^h, \text{ s.t.} \\ \left(\rho\ddot{\mathbf{u}}^h(t), \mathbf{v}^h\right)_\Omega + a_{\gamma_N}(\mathbf{u}^h(t), \mathbf{v}^h) + \left(\dfrac{1}{\gamma_N}\left[P_N(\mathbf{u}^h(t))\right]_{\mathbb{R}^-}, P_N(\mathbf{v}^h)\right)_{\Gamma_C} = l(t)(\mathbf{v}),\ \forall \mathbf{v}^h \in \mathbf{V}^h, k \end{cases} \tag{8}$$

where $a_{\gamma_N}(\mathbf{u}^h, \mathbf{v}^h) := a(\mathbf{u}^h, \mathbf{v}^h) - \left(\frac{1}{\gamma_N}\sigma_n(u^h), \sigma_n(v^h)\right)_{\Gamma_C}$. The notation $[\cdot]_{\mathbb{R}^-} := \min(0, \cdot)$ denotes the projection on the half-line formed by negative real numbers. The method is symmetric (non-symmetric and skew-symmetric versions also exist but are not considered here). Also, in static (or when $\rho = 0$), it is convergent and well-posed for γ_0 large enough. Subsequently, by using

Riesz's representation theorem, the mass operator $\mathbf{M} : \mathbf{V}^h \to \mathbf{V}^h$ and the nonlinear operator $\mathbf{B}_N : \mathbf{V}^h \to \mathbf{V}^h$ are defined such that

$$\begin{aligned} \Big(\mathbf{M}(\mathbf{v}^h), \mathbf{w}^h\Big)_\Omega &= \Big(\rho \mathbf{v}^h, \mathbf{w}^h\Big)_\Omega, \ \forall \mathbf{w}^h \in \mathbf{V}^h, \\ \Big(\mathbf{B}_N(\mathbf{v}^h), \mathbf{w}^h\Big)_{\Gamma_C} &= a_{\gamma_N}(\mathbf{v}^h, \mathbf{w}^h) + \left(\frac{1}{\gamma_N}\Big[P_N(\mathbf{v}^h)\Big]_{\mathbb{R}^-}, P_N(\mathbf{w}^h)\right)_{\Gamma_C}, \ \forall \mathbf{w}^h \in \mathbf{V}^h. \end{aligned} \tag{9}$$

The vector $\mathbf{L}(t) \in \mathbf{V}^h$ is then defined such that

$$\Big(\mathbf{L}(t), \mathbf{w}^h\Big)_\Omega = l(t)(\mathbf{w}^h), \ \forall \mathbf{w}^h \in \mathbf{V}^h. \tag{10}$$

Then, the compact form of (8) is

$$\begin{cases} \text{Seek } \mathbf{u}^h : [0,T] \to \mathbf{V}^h, \text{ s.t.} \\ \mathbf{M}\ddot{\mathbf{u}}^h(t) + \mathbf{B}_N(\mathbf{u}^h(t)) = \mathbf{L}(t), \\ \mathbf{u}^h(0) = \mathbf{u}_0^h, \quad \dot{\mathbf{u}}^h(0) = \dot{\mathbf{u}}_0^h, \end{cases} \tag{11}$$

which is a system of lipschitzien differential equations and its well-posedness has been proven in [19]. Let us define the discrete energy as follows:

$$E^h(t) := \frac{1}{2}\Big(\rho \dot{\mathbf{u}}^h(t), \dot{\mathbf{u}}^h(t)\Big)_\Omega + \frac{1}{2} a(\mathbf{u}^h(t), \mathbf{u}^h(t)), \tag{12}$$

which is associated to the solution $\mathbf{u}^h(t)$ to Problem (8). Note that this is the direct transposition of the mechanical energy $E(t)$ for the continuous system. Set also

$$\begin{aligned} E_N^h(t) &:= E^h(t) - \frac{1}{2}\Big|\Big|{\gamma_N}^{-\frac{1}{2}}\sigma_n(\mathbf{u}^h(t))\Big|\Big|_{\Gamma_C}^2 + \frac{1}{2}\Big|\Big|{\gamma_N}^{-\frac{1}{2}}\Big[P_N(\mathbf{u}^h(t))\Big]_{\mathbb{R}^-}\Big|\Big|_{\Gamma_C}^2 \\ &:= E^h(t) - R_N^h(t), \end{aligned} \tag{13}$$

which corresponds to a modified energy in which a consistent term is added. This term denoted $R_N^h(t)$ represents, roughly speaking, the nonfulfillment of the contact condition (1)(v) by $\mathbf{u}^h(t)$ [13, 19]. This modified energy E_N^h is conserved if (1) is conservative.

2.2 Penalty method

The discrete reformulation of the standard penalty method for the unilateral Signorini problem writes as follows:

$$\begin{cases} \text{Seek } \mathbf{u}_\epsilon^h : [0,T] \to \mathbf{V}^h, \text{ s.t.} \\ \Big(\rho \ddot{\mathbf{u}}_\epsilon^h(t), \mathbf{v}^h\Big)_\Omega + a(\mathbf{u}_\epsilon^h(t), \mathbf{v}^h) + \dfrac{1}{\epsilon}\left(\Big[u_{\epsilon,n}^h(t)\Big]_{\mathbb{R}+}, v_n^h\right)_{\Gamma_C} = l(t)(\mathbf{v}^h), \ \forall \mathbf{v} \in \mathbf{V}^h, \end{cases} \tag{14}$$

where $[\cdot]_{\mathbb{R}+} = \max(0, \cdot)$ denotes the projection on $\mathbb{R}+$, and $\epsilon_{|T\cap\Gamma_C} = \epsilon_0 h_T$ for each T intersected with Γ_C, with ϵ_0 a positive constant. This problem (14) is well-posed [7, 16] but is non-consistent, in contrast to Nitsche's method. There also exists a generalized class of penalty models applied to the Signorini problem, the so-called normal compliance model, corresponding to a power-law regularization of the penalty methods [10, 41, 50].

We can also define a compact form as for Nitsche's method:

$$\begin{cases} \text{Seek } \mathbf{u}_\epsilon^h : [0,T] \to \mathbf{V}^h \text{ s.t.} \\ \mathbf{M}\ddot{\mathbf{u}}_\epsilon^h(t) + \mathbf{B}_P(\mathbf{u}_\epsilon^h(t)) = \mathbf{L}(t), \\ \mathbf{u}_\epsilon^h(0) = \mathbf{u}_0^h, \quad \dot{\mathbf{u}}_\epsilon^h(0) = \dot{\mathbf{u}}_0^h, \end{cases} \tag{15}$$

with the nonlinear operator $\mathbf{B}_P : \mathbf{V}^h \to \mathbf{V}^h$ defined using Riesz's theorem:

$$\left(\mathbf{B}_P(\mathbf{v}^h), \mathbf{w}^h\right)_{\Gamma_C} = a(\mathbf{v}^h, \mathbf{w}^h) + \left(\frac{1}{\epsilon}\left[v_n^h\right]_{\mathbb{R}+}, w_n^h\right)_{\Gamma_C}, \ \forall \mathbf{w} \in \mathbf{V}^h. \tag{16}$$

The modified energy associated with the penalty method is the following one [23, 32]:

$$E_P^h(t) := E^h(t) + \frac{1}{2}\left|\left|\epsilon^{-\frac{1}{2}}\left[u_n^h(t)\right]_{\mathbb{R}+}\right|\right|_{\Gamma_C}^2. \tag{17}$$

2.3 Augmented Lagrangian

The augmented Lagrangian method has been proposed as a penalty-duality formulation [1]. We first introduce the bi-linear form $P_A(\mathbf{u}, \lambda) = \lambda - \gamma_A u_n$, and the contact pressure can be reformulated as $\lambda = [P_A(\mathbf{u}, \lambda)]_{\mathbb{R}^-}$ [59], where γ_A is a positive parameter. In this work, γ_A is taken similarly to γ_N as $\gamma_{A|T\cap\Gamma_C} = \frac{\gamma_a}{h_T}$ for each T intersected with Γ_C and with γ_a a positive constant. Different formulations for contact problems in the static case have been introduced [8]. In this work, we focus on the following augmented Lagrangian reformulation:

$$\begin{cases} \text{Seek } (\mathbf{u}^h, \lambda^h) : [0,T] \to \mathbf{V}^h \times W^h, \text{ s.t.} \\ \left(\rho\ddot{\mathbf{u}}^h(t), \mathbf{v}^h\right)_\Omega + a(\mathbf{u}^h(t), \mathbf{v}^h) - \left(\left[P_A(\mathbf{u}^h(t), \lambda^h(t))\right]_{\mathbb{R}^-}, v_n^h\right)_{\Gamma_C} = l(t)(\mathbf{v}^h), \quad \forall \mathbf{v}^h \in \mathbf{V}^h, \\ \left(\frac{1}{\gamma_A}\left(\left[P_A(\mathbf{u}^h(t), \lambda^h(t))\right]_{\mathbb{R}^-} - \lambda^h(t)\right), \mu^h\right)_{\Gamma_C} = 0, \qquad \forall \mu^h \in W^h. \end{cases} \tag{18}$$

The stability of (18) with conditions in the static case (or when $\rho = 0$) for a scalar field has been proven by [8, Sect. 4]. This reformulation is also known as the proximal ALM, and the relation with Nitsche's method (8) can be obtained by interpreting λ^h as $\sigma_n(\mathbf{u}^h)$.

Similar to Nitsche's method and the penalty method, we can write a compact form:

$$\begin{cases} \text{Seek } (\mathbf{u}^h, \lambda^h) : [0,T] \to \mathbf{V}^h \times W^h \text{ s.t.} \\ \mathbf{M}\ddot{\mathbf{u}}^h(t) + \mathbf{B}_A(\mathbf{u}^h(t), \lambda^h(t)) = \mathbf{L}(t), \\ \mathbf{u}^h(0) = \mathbf{u}_0^h, \quad \dot{\mathbf{u}}^h(0) = \dot{\mathbf{u}}_0^h, \end{cases} \tag{19}$$

with nonlinear operator $\mathbf{B}_A : \mathbf{V}^h \times W^h \to \mathbf{V}^h \times W^h$ defined using Riesz's theorem:

$$\begin{aligned}\Big(\mathbf{B}_A(\mathbf{v}^h,\mu^h),(\mathbf{w}^h,\xi^h)\Big)_{\Gamma_C} = a(\mathbf{v}^h,\mathbf{w}^h) + \left(\frac{1}{\gamma_A}\left[P_A(\mathbf{v}^h,\mu^h)\right]_{\mathbb{R}-}, P_A(\mathbf{w}^h,\xi^h)\right)_{\Gamma_C} \\ - \left(\frac{1}{\gamma_A}\mu^h,\xi^h\right)_{\Gamma_C},\ \forall\ (\mathbf{w}^h,\xi^h)\in\mathbf{V}^h\times W^h.\end{aligned} \tag{20}$$

The modified energy $E_L^h(t)$ can be set as:

$$\begin{aligned}E_L^h(t) &:= E^h(t) - \frac{1}{2}\left|\left|{\gamma_A}^{-\frac{1}{2}}\lambda^h(t)\right|\right|^2_{\Gamma_C} + \frac{1}{2}\left|\left|{\gamma_A}^{-\frac{1}{2}}\left[P_A(\mathbf{u}^h(t),\lambda^h(t))\right]_{\mathbb{R}^-}\right|\right|^2_{\Gamma_C} \\ &:= E^h(t) - R_L^h(t).\end{aligned} \tag{21}$$

2.4 Elastodynamic and mass redistribution method

For penalty or Nitsche's method, we have the semi-discrete problem defined in the form

$$\begin{cases}\text{Seek } \mathbf{u}^h : [0,T]\to\mathbf{V}^h \text{ s.t.}\\ \mathbf{M}\ddot{\mathbf{u}}^h(t) + \mathbf{B}(\mathbf{u}^h(t)) = \mathbf{L}(t),\\ \mathbf{u}^h(0) = \mathbf{u}_0^h, \quad \dot{\mathbf{u}}^h(0) = \dot{\mathbf{u}}_0^h,\end{cases} \tag{22}$$

where $\mathbf{B}$ is equal to $\mathbf{B}_P$, or $\mathbf{B}_N$, for penalty, or Nitsche's method, respectively. And, for ALM:

$$\begin{cases}\text{Seek } (\mathbf{u}^h,\lambda^h) : [0,T]\to\mathbf{V}^h\times W^h \text{ s.t.}\\ \mathbf{M}\ddot{\mathbf{u}}^h(t) + \mathbf{B}_A(\mathbf{u}^h(t),\lambda^h(t)) = \mathbf{L}(t),\\ \mathbf{u}^h(0) = \mathbf{u}_0^h, \quad \dot{\mathbf{u}}^h(0) = \dot{\mathbf{u}}_0^h\end{cases} \tag{23}$$

A large part of the numerical instabilities for simulations of dynamic contact problems come from the strong discontinuity of acceleration at the contact boundary. A novel idea is the mass redistribution method which conserves the total mass, the center of gravity, and the inertia momenta, but is built so that there is no inertia for the contact nodes [25, 39]. Moreover, the redistributed mass matrix $\mathbf{M}^r$ has the same form as $\mathbf{M}$, *i.e.*, the zeros are in the same positions for the two matrices [39, Sect. 4.1]. An example of a comparison of different mass matrices on a 1D bar occupying $\Omega = [0,1]$ meshed uniformly with 20 linear elements is illustrated in Fig. 2, with contact boundary at $x = 0$ and Dirichlet boundary at $x = 1$. Each cross represents a node with its mass valued on the y-axis: the mass is uniformly distributed (except the two nodes on the two sides which possess only half as in the middle); while for redistributed mass matrix, the node at $x = 0$ has a zero-mass and its initial mass has been redistributed to other nodes.

3 Discretization in time

In this work, we are especially interested in two families of time-marching schemes: the HHT-α scheme and the TR-BDF2 schemes.

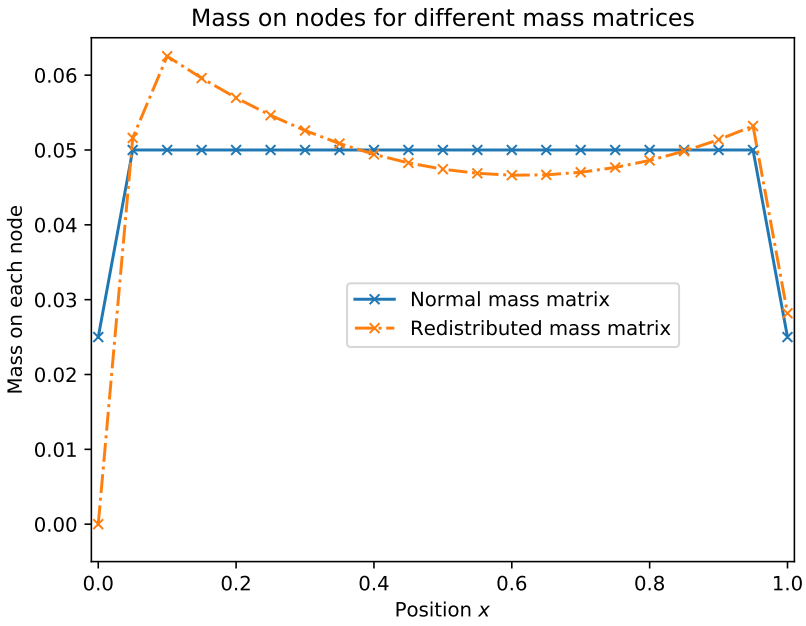

Figure 2: Comparison of different mass matrices on linear 1D elements.

3.1 Hilber-Hughes-Taylor-α (HHT-α) scheme

The HHT-α scheme [34] is a classical scheme for elastodynamic problems. Let $\Delta t > 0$ be the time-step and consider a uniform discretization of the time interval $[0, T] : (t^0, \cdots, t^N)$, with $t^n = n\Delta t, n = 0, \cdots, N$. This scheme consists in solving a nonlinear problem for each time instant t^{n+1} using the displacement $\mathbf{u}^{h,n}$, velocity $\dot{\mathbf{u}}^{h,n}$, and acceleration $\ddot{\mathbf{u}}^{h,n}$ of instant t^n as known variables:

$$\begin{cases} \text{Seek } \mathbf{u}^{h,n+1}, \dot{\mathbf{u}}^{h,n+1}, \ddot{\mathbf{u}}^{h,n+1} \in \mathbf{V}^h \text{ s.t.} \\ \mathbf{u}^{h,n+1} = \mathbf{u}^{h,n} + \Delta t \dot{\mathbf{u}}^{h,n} + \dfrac{\Delta t^2}{2}((1-2\tilde{\beta})\ddot{\mathbf{u}}^{h,n} + 2\tilde{\beta}\ddot{\mathbf{u}}^{h,n+1}), & \text{(i)} \\ \dot{\mathbf{u}}^{h,n+1} = \dot{\mathbf{u}}^{h,n} + \Delta t((1-\tilde{\gamma})\ddot{\mathbf{u}}^{h,n} + \tilde{\gamma}\ddot{\mathbf{u}}^{h,n+1}), & \text{(ii)} \\ \mathbf{M}\ddot{\mathbf{u}}^{h,n+1} + (1-\tilde{\alpha})\mathbf{B}(\mathbf{u}^{h,n+1}) + \tilde{\alpha}\mathbf{B}(\mathbf{u}^{h,n}) = (1-\tilde{\alpha})\mathbf{L}^{n+1} + \tilde{\alpha}\mathbf{L}^n, & \text{(iii)} \end{cases} \tag{24}$$

where $\mathbf{u}^{h,n+1}, \dot{\mathbf{u}}^{h,n+1}$, and $\ddot{\mathbf{u}}^{h,n+1}$ are the displacement, velocity, and acceleration to be solved. The parameter $\tilde{\alpha}$ allows a dissipation for high frequencies. The scheme parameters $(\tilde{\alpha}, \tilde{\beta}, \tilde{\gamma})$ are often related in practice. A classical combination of the parameters is $\tilde{\alpha} \in \left[0, \frac{1}{3}\right], \tilde{\beta} = \frac{1}{4}(1+\tilde{\alpha})^2, \tilde{\gamma} = \frac{1}{2} + \tilde{\alpha}$. Such a choice of parameters yields unconditional stability for linear elasticity and the scheme is implicit. Notably, for $\tilde{\alpha} = 0$, the scheme is also known as the Crank-Nicolson scheme or a scheme of the Newmark family with $\tilde{\beta} = \frac{1}{4}$ and $\tilde{\gamma} = \frac{1}{2}$ (or the implicit

trapezoidal method). In this case, the scheme conserves the energy in the linear elastic domain without contact and has a second-order accuracy. But with the presence of contact, it can be more complicated and can introduce additional oscillations and numerical energy [20].

Larger values of $\tilde{\alpha}$ help filter more oscillation on high frequencies, however, it dissipates also more energy so we might lose the reliability at an industrial point. We would like to provide a possible value of the parameter that allows an acceptable compromise between parasitic oscillation and the loss of energy.

3.2 Possibility of opposed parameter

A positive value for the parameter $\tilde{\alpha}$ (with $\tilde{\beta} = \frac{1}{4}(1 + |\tilde{\alpha}|)^2$ and $\tilde{\gamma} = \frac{1}{2} + |\tilde{\alpha}|$ in order to keep the values of $\tilde{\beta}$ and $\tilde{\gamma}$ remaining in the unconditionally stable region), representing an interpolation of the external and internal force can provide dissipation of energy of high frequencies. Moreover, we found that an extrapolation realized with a negative value can also provide a similar effect. We detail this point below with a stability and consistency analysis. Consider a single-degree-of-freedom (SDOF) oscillator

$$\begin{cases} m\ddot{u} + ku = 0, t \in (0, T), \\ u(0) = u^0, \dot{u}(0) = \dot{u}^0. \end{cases} \tag{25}$$

Let $u = u(t)$ be the exact solution and $u^n, \dot{u}^n, \ddot{u}^n$ the approximate values at time $t^n = n\Delta t, n \in \mathbb{N}$. For a one-step method, we can define a corresponding continuous operator $\Phi_{\Delta t} : [0, T] \times \mathbb{R}^3 \to \mathbb{R}$ depending on the time-step Δt, [60] so that u^{n+1} can be calculated by:

$$u^{n+1} = u^n + \Delta t \Phi_{\Delta t}(t^n, u^n, \dot{u}^n, \ddot{u}^n), \tag{26}$$

and the associated local truncation error [36, 57, 60] is:

$$T_n := \frac{u(t^{n+1}) - u(t^n)}{\Delta t} - \Phi_{\Delta t}(t^n, u(t^n), \dot{u}(t^n), \ddot{u}(t^n)). \tag{27}$$

Applying to the SDOF system (25), the error is then bounded (see Sect. A.1 for details):

$$\begin{aligned} |T_n| &\leq \tilde{\beta} \left|\omega^2 u(t^n) + \ddot{u}(t^n)\right| \Delta t + \tilde{\beta} \left(1 - \tilde{\alpha}\right) \omega^2 \left|\dot{u}(t^n)\right| \Delta t^2 + O(\Delta t^2) \\ &= \tilde{\beta} \left(1 - \tilde{\alpha}\right) \omega^2 \left|\dot{u}(t^n)\right| \Delta t^2 + O(\Delta t^2), \end{aligned} \tag{28}$$

with $\omega^2 = \frac{k}{m}$. And a second-order convergence is achieved.

3.2.1 Analysis of spectral radius

Let us rewrite the discrete problem of system (25) in matrix form (see Sect. A.2 for the expression of matrix $\mathbf{A}$):

$$\mathbf{Y}^{n+1} = \mathbf{A}\mathbf{Y}^n, \tag{29}$$

where $\mathbf{Y}^n = [u^n, \Delta t \dot{u}^n, \Delta t^2 \ddot{u}^n]^T$ and $\mathbf{A}$ the amplification matrix. The spectral radius of $\mathbf{A}$ is defined by:

$$\rho(\mathbf{A}) = \max_{1 \leq i \leq 3} |\lambda_i|, \tag{30}$$

where $\lambda_i, i \in \{1, 2, 3\}$, are the eigenvalues of $\mathbf{A}$. The condition $\rho(\mathbf{A}) \leq 1$ is equivalent to the unconditional stability of the scheme irrespectively to the time-step, for linear boundary conditions.

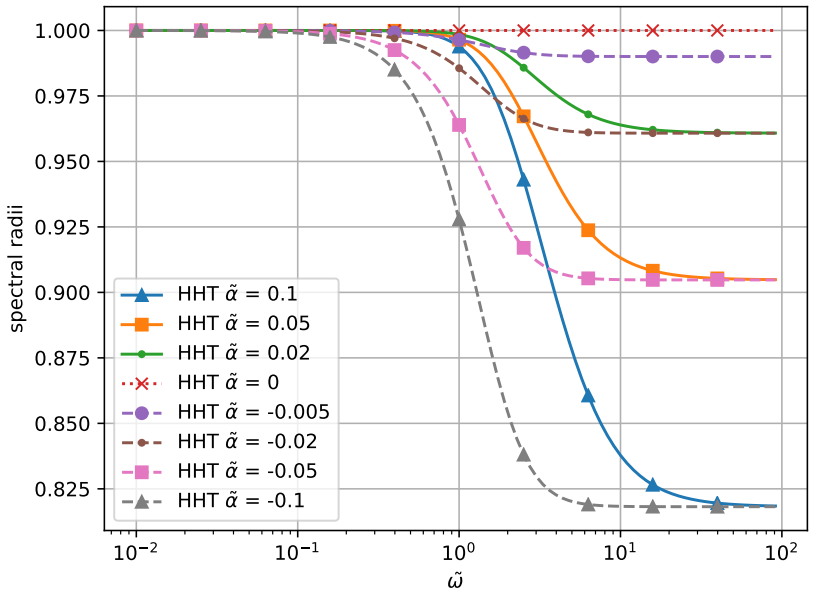

Figure 3: Spectral radii for HHT-α scheme vs frequencies for different $\tilde{\alpha}$.

We illustrate the spectral radii for the HHT-α scheme with different values of parameter $\tilde{\alpha}$ in Fig.3. The spectral radii show a dissipation for high frequencies and a negative $\tilde{\alpha}$ dissipates more at lower frequencies than its positive counterpart. Moreover, it can be observed that the spectral radii tend to have the same value when $\tilde{\omega} := \omega^2 \Delta t^2 \to \infty$ for opposite $\tilde{\alpha}$ but with the same absolute value. In fact, when $\tilde{\omega} \to \infty$,

$$\lim_{\tilde{\omega} \to \infty} \mathbf{A} = \begin{bmatrix} \frac{-\tilde{\alpha}}{1-\tilde{\alpha}} & 0 & 0 \\ \frac{\tilde{\gamma}}{\tilde{\beta}} \left(\frac{-\tilde{\alpha}}{1-\tilde{\alpha}} \right) & 1 - \frac{\tilde{\gamma}}{\tilde{\beta}} & 1 - \frac{\tilde{\gamma}}{2\tilde{\beta}} \\ \frac{1}{\tilde{\beta}} \left(\frac{-\tilde{\alpha}}{1-\tilde{\alpha}} \right) & -\frac{1}{\tilde{\beta}} & \frac{2\tilde{\beta}-1}{2\tilde{\beta}} \end{bmatrix}, \tag{31}$$

which has the following eigenvalues:

$$\begin{cases} \lambda_1 = \dfrac{-\tilde{\alpha}}{1-\tilde{\alpha}}, \\ \lambda_2 = \dfrac{4\tilde{\beta}-2\tilde{\gamma}-1}{4\tilde{\beta}} - \sqrt{\dfrac{-16\tilde{\beta}+4\tilde{\gamma}^2+4\tilde{\gamma}+1}{4\tilde{\beta}}}, \\ \lambda_3 = \dfrac{4\tilde{\beta}-2\tilde{\gamma}-1}{4\tilde{\beta}} + \sqrt{\dfrac{-16\tilde{\beta}+4\tilde{\gamma}^2+4\tilde{\gamma}+1}{4\tilde{\beta}}}. \end{cases} \tag{32}$$

With respect to the relation between $\tilde{\alpha}$, $\tilde{\beta}$ and $\tilde{\gamma}$, we have $-16\tilde{\beta}+4\tilde{\gamma}^2+4\tilde{\gamma}+1=0$, and thus $\lambda_2=\lambda_3=\frac{4\tilde{\beta}-2\tilde{\gamma}-1}{4\tilde{\beta}}$ and $\lim_{\tilde{\omega}\to\infty}\rho(\mathbf{A})=|\lambda_2|=\frac{1-|\tilde{\alpha}|^2}{(1+|\tilde{\alpha}|)^2}$, for $\tilde{\alpha}\in[-\frac{1}{3},\frac{1}{3}]$.

3.3 TR-BDF2 scheme

In recent years, more and more research has been achieved on schemes with multiple sub-steps. Among them, we have several popular ones such as the TR-BDF2 scheme [3, 4, 35, 47] (also known as the Bathe scheme in some contexts). This scheme is a predictor-corrector scheme that uses the implicit trapezoidal rule (Crank-Nicolson) for the first sub-step by taking $\tilde{\gamma}\Delta t$ as the step and the second-order backward differentiation formula for the second one, using the data at t^n and calculated previously for the first sub-step.

$$\begin{cases} \text{Seek } \mathbf{u}^{h,n+1}, \dot{\mathbf{u}}^{h,n+1}, \ddot{\mathbf{u}}^{h,n+1} \in \mathbf{V}^h \text{ s.t.} \\ \tilde{\dot{\mathbf{u}}}^{h,n+\tilde{\gamma}} = \dot{\mathbf{u}}^{h,n} + \dfrac{\tilde{\gamma}\Delta t}{2}\left(\ddot{\mathbf{u}}^{h,n} + \tilde{\ddot{\mathbf{u}}}^{h,n+\tilde{\gamma}}\right), & \text{(i)} \\ \tilde{\mathbf{u}}^{h,n+\tilde{\gamma}} = \mathbf{u}^{h,n} + \tilde{\gamma}\Delta t\mathbf{v}^{h,n} + \dfrac{\tilde{\gamma}^2\Delta t^2}{4}\left(\ddot{\mathbf{u}}^{h,n} + \tilde{\ddot{\mathbf{u}}}^{h,n+\tilde{\gamma}}\right), & \text{(ii)} \\ \mathbf{M}\tilde{\ddot{\mathbf{u}}}^{h,n+\tilde{\gamma}} + \mathbf{B}\tilde{\mathbf{u}}^{h,n+\tilde{\gamma}} = \mathbf{L}^{n+\tilde{\gamma}}, & \text{(iii)} \\ \dot{\mathbf{u}}^{h,n+1} = \dfrac{1}{\tilde{\gamma}(2-\tilde{\gamma})}\tilde{\dot{\mathbf{u}}}^{h,n+\tilde{\gamma}} - \dfrac{(1-\tilde{\gamma})^2}{\tilde{\gamma}(2-\tilde{\gamma})}\dot{\mathbf{u}}^{h,n} + \dfrac{1-\tilde{\gamma}}{2-\tilde{\gamma}}\Delta t\ddot{\mathbf{u}}^{h,n+1}, & \text{(iv)} \\ \mathbf{u}^{h,n+1} = \dfrac{1}{\tilde{\gamma}(2-\tilde{\gamma})}\tilde{\mathbf{u}}^{h,n+\tilde{\gamma}} - \dfrac{(1-\tilde{\gamma})^2}{\tilde{\gamma}(2-\tilde{\gamma})}\mathbf{u}^{h,n} + \dfrac{1-\tilde{\gamma}}{2-\tilde{\gamma}}\Delta t\dot{\mathbf{u}}^{h,n+1}, & \text{(v)} \\ \mathbf{M}\ddot{\mathbf{u}}^{h,n+1} + \mathbf{B}\mathbf{u}^{h,n+1} = \mathbf{L}^{n+1}. & \text{(vi)} \end{cases} \tag{33}$$

A popular value for the parameter $\tilde{\gamma}$ can be taken as $2-\sqrt{2}$, in which case, the linear systems at the two sub-steps are identical for linear elasticity. This scheme is also dissipative. We define the amplification matrix and its spectral radius similarly and illustrate in Fig. 4 for $\tilde{\gamma}=2-\sqrt{2}$. This scheme is highly dissipative compared to the HHT-α scheme.

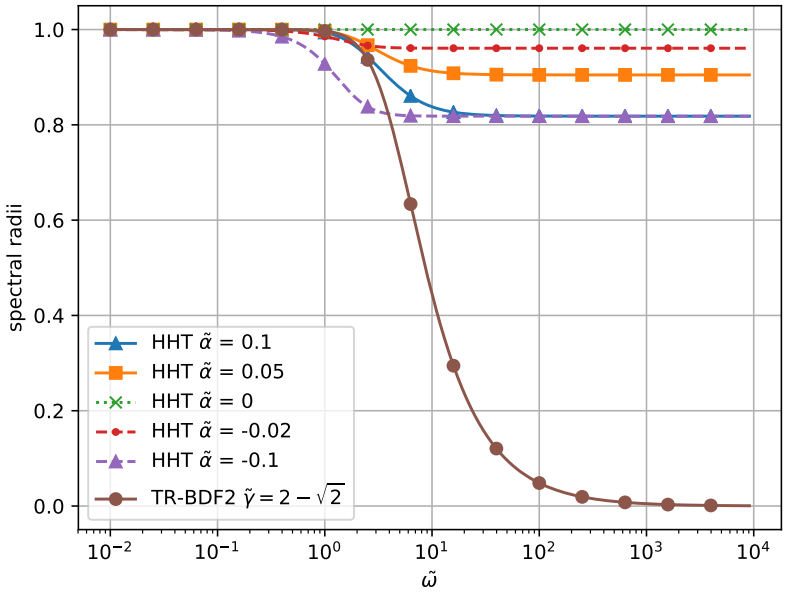

Figure 4: Spectral radii for HHT-α and TR-BDF2 schemes.

4 Numerical simulation

In this section, the numerical results for three different benchmarks (two uni-dimensional elastic problems and the bounce of a sphere) involving unilateral contact with a rigid obstacle are illustrated. In each simulation, the discrete modified energy will be displayed. For the two 1D tests, Nitsche's and penalty methods are combined with HHT-α and TR-BDF2 schemes. For the last test, Nitsche's and ALM are combined with HHT-α and TR-BDF2 schemes, and the Nitsche hybrid scheme [20] has also been applied. The nonlinear equations in each scheme (24)-(iii), (33)-(iii) and (vi) are solved by the semi-smooth Newton's method [55]. Moreover, the standard mass and mass redistribution methods are also compared. All numerical simulations are realized via finite element software GetFEM [56] using the Python interface.

4.1 1D elastic bar with Signorini and Dirichlet boundary conditions

In this section, we consider the test case proposed in [25, Sect. 5] and named 1D-SD in what follows. The 1D bar is the solution to the following dynamic equilibrium problem:

$$\begin{cases} \text{Seek } u(x,t) : [0,1] \times (0,T) \to \mathbb{R} \text{ s.t.} \\ \dfrac{\partial^2 u}{\partial t^2} - \dfrac{\partial^2 u}{\partial x^2} = 0, \\ u(1,t) = 0, \\ u(0,t) \geq 0, \dfrac{\partial u}{\partial x}(0,t) \leq 0, u(0,t)\dfrac{\partial u}{\partial x}(0,t) = 0, \\ u(x,0) = \dfrac{1}{2} - \dfrac{x}{2}, \dfrac{\partial u}{\partial t}(x,0) = 0. \end{cases} \tag{34}$$

The deformation of the bar at different times is illustrated in Fig. 5. Both a constant mesh size $h = 0.05$ and time step $\Delta t = 0.05$ are used. The Nitsche's parameter γ_0 and the penalty parameter ϵ_0 are chosen to be identical $\gamma_0 = \frac{1}{\epsilon_0} = 5$.

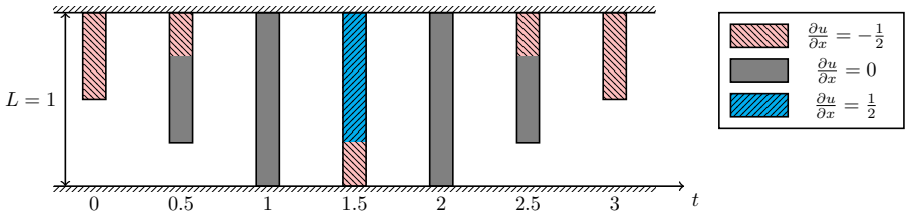

Figure 5: 1D-SD: Deformation of the bar at different times.

4.1.1 Crank-Nicolson scheme ($\tilde{\alpha} = 0$)

Firstly, the Crank-Nicolson scheme (HHT-α method with $\tilde{\alpha} = 0$) is used and is considered as a referral scheme to study the effect of numerical dissipation. The numerical and analytical solutions are displayed in Fig. 6. From up to down, the displacement and the velocity at the contact point ($x = 0$), the contact pressure, and the numerical energy are plotted. It is observed that there is penetration on Γ_C for the penalty method as expected since it is non-consistent, while with Nitsche's method the penetration observed is much less. More oscillations are observed with the standard mass method except for the velocity. The redistributed mass allows more regular solutions on displacement and especially on contact pressure; however, with a mass-free node at the endpoint, an oscillation in velocity caused by an initial perturbation occurs and holds for non-dissipative schemes. This supplementary oscillation can be limited over time by dissipative schemes shown in the following paragraphs. Moreover, spurious oscillations on the velocity are related to the continuous approximation in the space with Lagrange finite elements, which is not adapted to handle shocks.

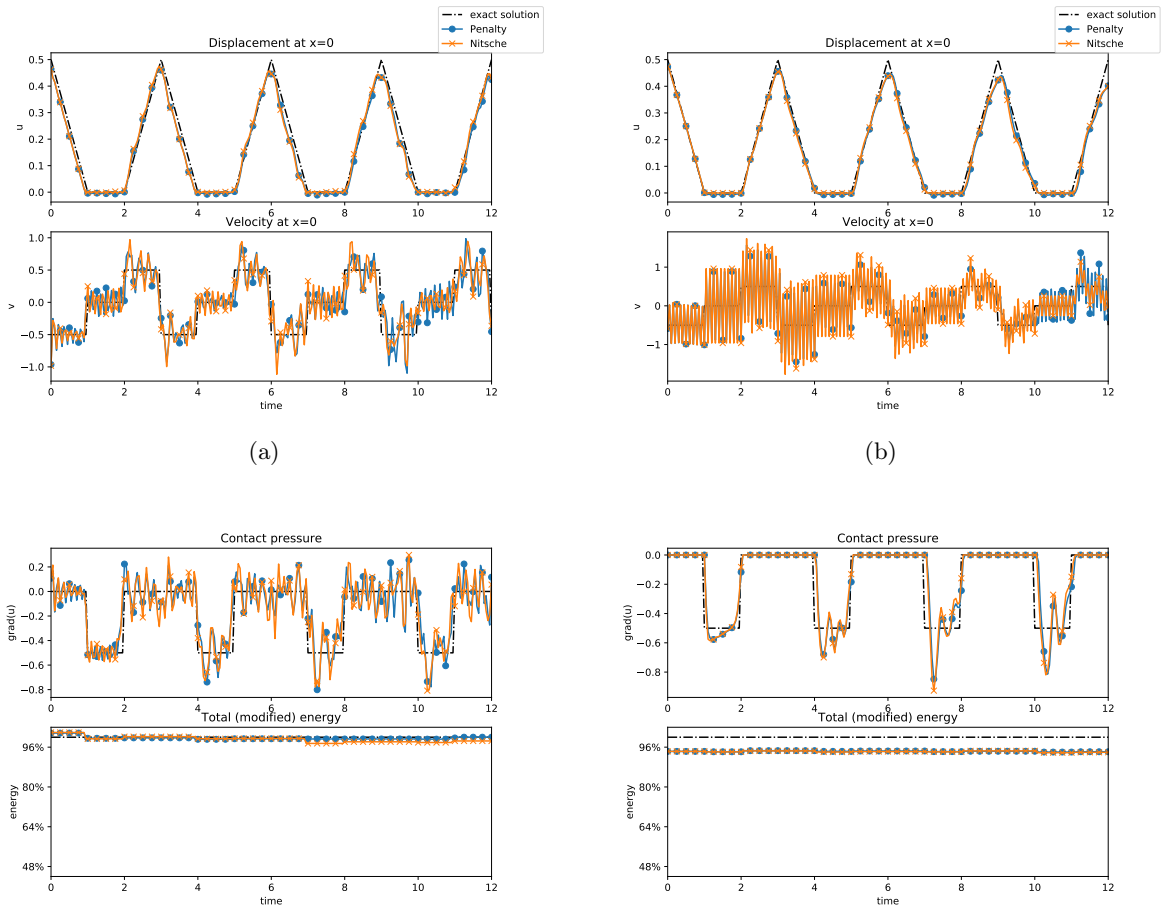

Figure 6: 1D-SD: Comparison of the analytical solution and the numerical solutions for standard (left) and modified (right) mass matrices with the Crank-Nicolson scheme ($\tilde{\alpha} = 0$).

4.1.2 HHT-α scheme

The results for the HHT-α scheme with parameter $\tilde{\alpha} \in \{0.05, -0.02\}$ are illustrated in Fig. 7. A non-zero $\tilde{\alpha}$ helps to dissipate high-frequency oscillations as described in Sect. 3.1. More regular displacements are observed compared with those obtained with the Crank-Nicolson scheme. With the redistributed mass, the contact pressure maintains zero during non-contact phases but an important initial oscillation in velocity is observed. For a negative value $\tilde{\alpha} = -0.02$, as the dissipation starts at a lower frequency, we obtain a more regular solution but with more loss of energy. The loss of energy can be important with a negative but with a higher magnitude value of $\tilde{\alpha}$, so its value should be chosen cautiously in order to guarantee the reliability of numerical

results. The value, for instance, $\tilde{\alpha} = -0.02$ provides a compromise between energy dissipation and oscillations.

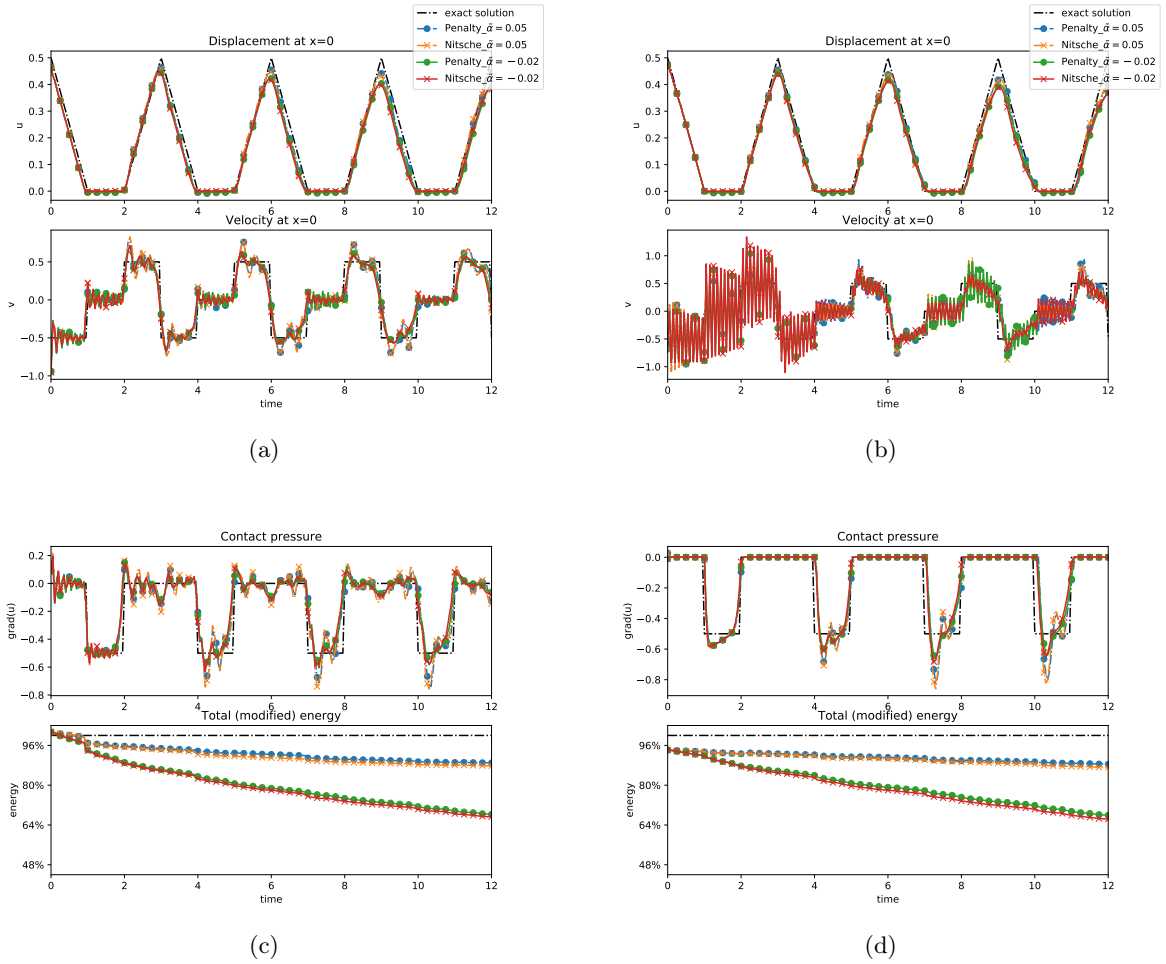

Figure 7: 1D-SD: Comparison of the analytical and discrete solutions for the standard (left) and modified (right) mass matrices with HHT-α method and $\tilde{\alpha} \in \{0.05, -0.02\}$.

4.1.3 TR-BDF2 scheme

The plots for TR-BDF2 scheme with $\tilde{\gamma} = 2 - \sqrt{2}$ are shown in Fig. 8. Fewer oscillations and energy dissipation are observed for TR-BDF2 than for HHT-α, especially for the redistributed mass method where the corrector step helps to reduce the oscillation on velocity (see Fig. 8b).

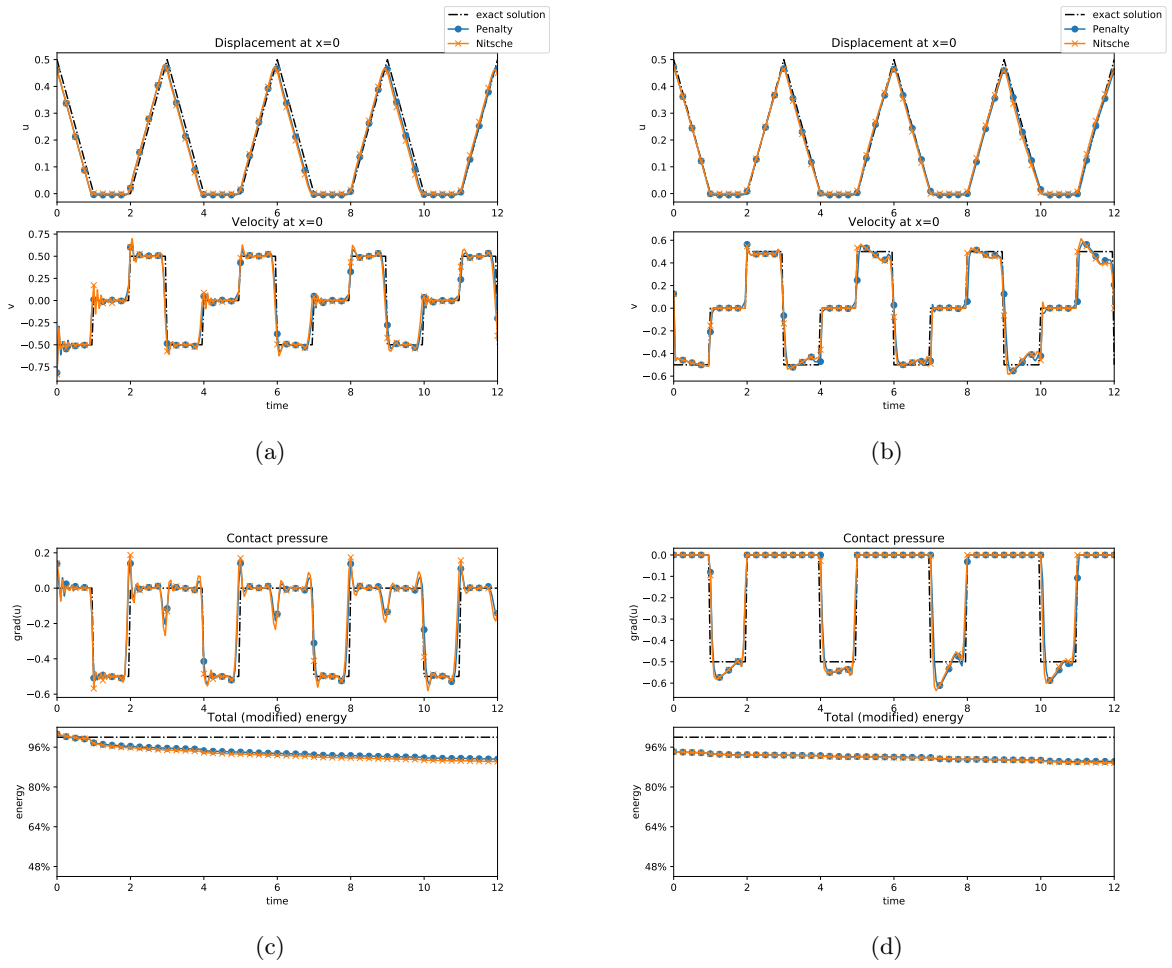

Figure 8: 1D-SD: Comparison of the analytical solution and discrete solutions for standard (left) and modified (right) mass matrices with TRBDF2 scheme.

4.1.4 Numerical convergence

In this test of convergence, variant mesh sizes and time steps are applied by fixing the ratio $\frac{\Delta t}{h} = 1$. The errors on $L^2(0,T;H^1(\Omega))$-norm are illustrated in Fig. 9. Similar convergence order is observed for the HHT-α scheme with different values of parameter $\tilde{\alpha}$.

4.2 1D elastic bar with two Signorini boundary conditions

We propose here a new benchmark with an analytical solution: a 1D elastic bar with two rigid obstacles (at $x = 0$ and at $x = 1.5$) and is called 1D-SS in what follows. The bar is initially compressed to half-high and has a constant velocity $v_0 = -\frac{1}{2}$. The benchmark consists to solve

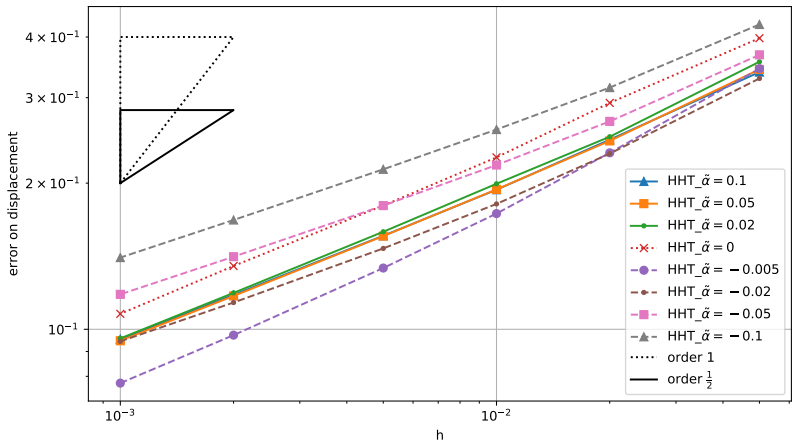

Figure 9: L^2H^1-error vs h with $\frac{\Delta t}{h} = 1$.

the problem (35):

$$\begin{cases} \text{Seek } u(x,t) : [0,1] \times (0,T) \to \mathbb{R}, \text{ s.t.} \\ \dfrac{\partial^2 u}{\partial t^2} - \dfrac{\partial^2 u}{\partial x^2} = 0, \\ u(0,t) \geq 0, \ \dfrac{\partial u}{\partial x}(0,t) \leq 0, \ u(0,t)\dfrac{\partial u}{\partial x}(0,t) = 0, \\ u(1,t) \leq \dfrac{1}{2}, \ \dfrac{\partial u}{\partial x}(1,t) \leq 0, \ \left(u(1,t) - \dfrac{1}{2}\right)\dfrac{\partial u}{\partial x}(1,t) = 0, \\ u(x,0) = 1 - \dfrac{x}{2}, \ \dfrac{\partial u}{\partial t}(x,0) = -\dfrac{1}{2}. \end{cases} \tag{35}$$

The analytical solution is piecewise regular and periodic. The movement of the elastic bar (displaced position over time) is shown in Fig. 10 and the analytical solution is illustrated on the $x-t$ diagram in Fig. 11. The impact of each side has three different states: 1. non-contact; 2. contact with a zero contact pressure; 3. contact with a contact pressure non-zero. The most interesting part of the benchmark locates at state 2, contact with a zero contact pressure state, *e.g.* for the side $x = 0$ when $t \in [1, 2]$. As mentioned in [21], the situation called "grazing contact" (both $u_n = 0$ and $\frac{\partial u}{\partial x} = 0$ on Γ_C) is a non-differentiable case for operators $\mathbf{B}_N$ and $\mathbf{B}_A$.

The same combination of contact methods and time schemes as for Sect. 4.1 is used; and with the following parameters: mesh size $h = 0.05$, the time step $\Delta t = 0.05$, and $\gamma_0 = \frac{1}{\epsilon_0} = 5$. The mass redistribution method implies here that the mass is eliminated at both sides of the bar.

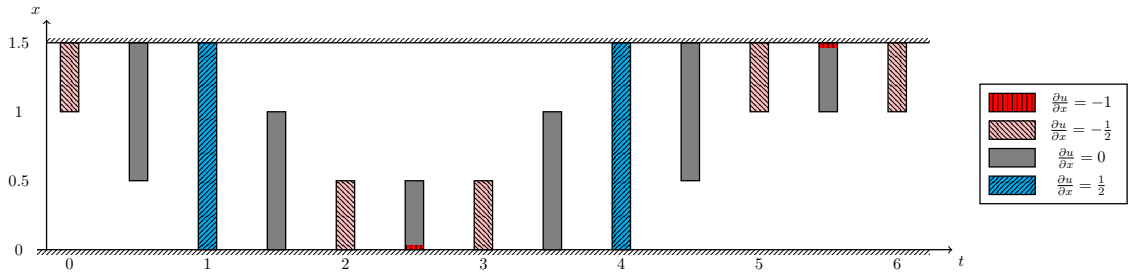

Figure 10: 1D-SS: "Wriggle" between two rigid obstacles.

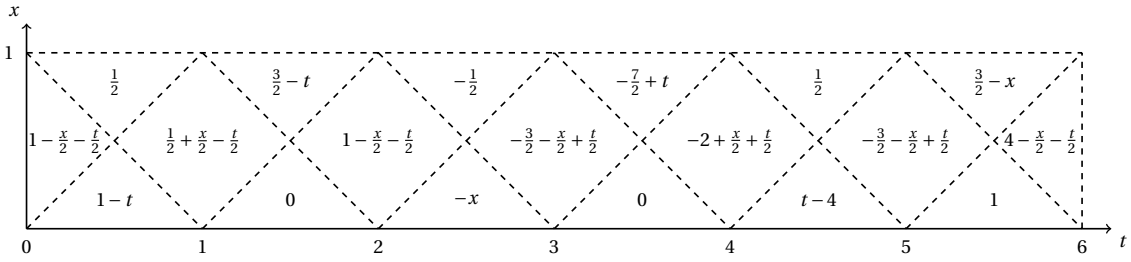

Figure 11: 1D-SS: Displacement in each region of the $x - t$ diagram.

4.2.1 Crank-Nicolson scheme ($\tilde{\alpha} = 0$)

The results obtained for the Crank-Nicolson scheme are shown in Fig. 12. Oscillations can be observed since the method is non-dissipative with the standard mass method. As with the modified mass method, the displacement and contact pressure are more regular and the oscillations are important for velocity caused by the initial perturbation. As this new benchmark contains no Dirichlet boundary condition, the whole system is on a free vibration coupled with contact on two sides, which makes the benchmark more complicated for numerical simulation.

4.2.2 HHT-α scheme

The numerical results for the HHT-α scheme with $\tilde{\alpha} \in \{0.05, -0.02\}$ are shown in Fig. 13. As expected, dissipation at high frequencies is observed. Moreover, as before, less oscillation is present for $\tilde{\alpha} = -0.02$ than for $\tilde{\alpha} = 0.05$ but the dissipation is higher. Once again, this value gives an interesting compromise between oscillation and energy dissipation; especially with the modified mass method.

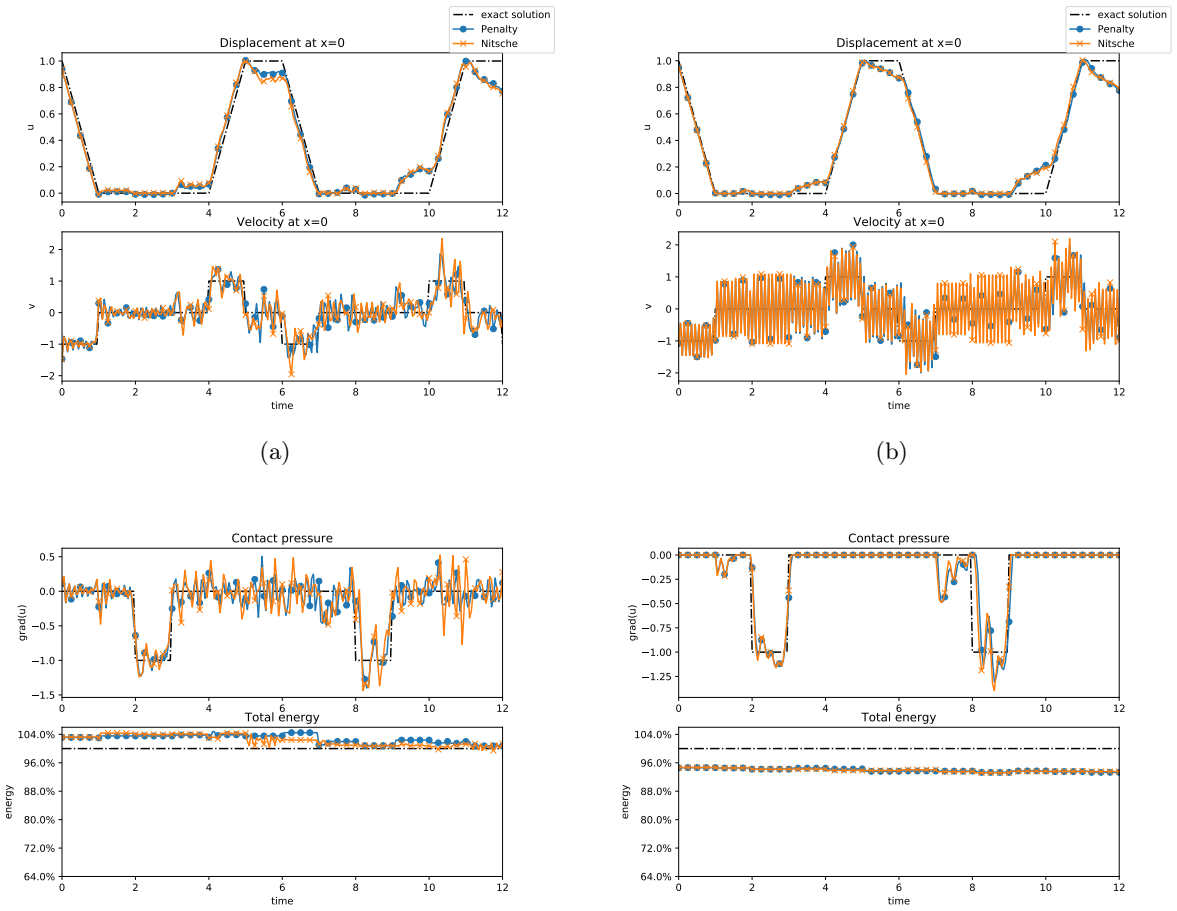

Figure 12: 1D-SS: Comparison of the analytical and discrete solutions for standard (left) and modified (right) mass matrices with the Crank-Nicolson method.

4.2.3 TR-BDF2 scheme

The TR-BDF2 scheme is used with $\tilde{\gamma} = 2 - \sqrt{2}$ in Fig. 14. As expected, the results are better with this 2-step predictor-corrector scheme compared to the HHT-α scheme. As before, the modified mass method has less oscillation than the standard one.

4.3 3D impact of a sphere

The last benchmark is a three-dimensional sphere which impacts a rigid foundation at $z = 0$. The center of the sphere is initially at $[0, 0, 2]^T$ with zero initial velocity and has a diameter $D = 40$. The mesh used is a second-order tetrahedron mesh with $h = 4$ and a constant time

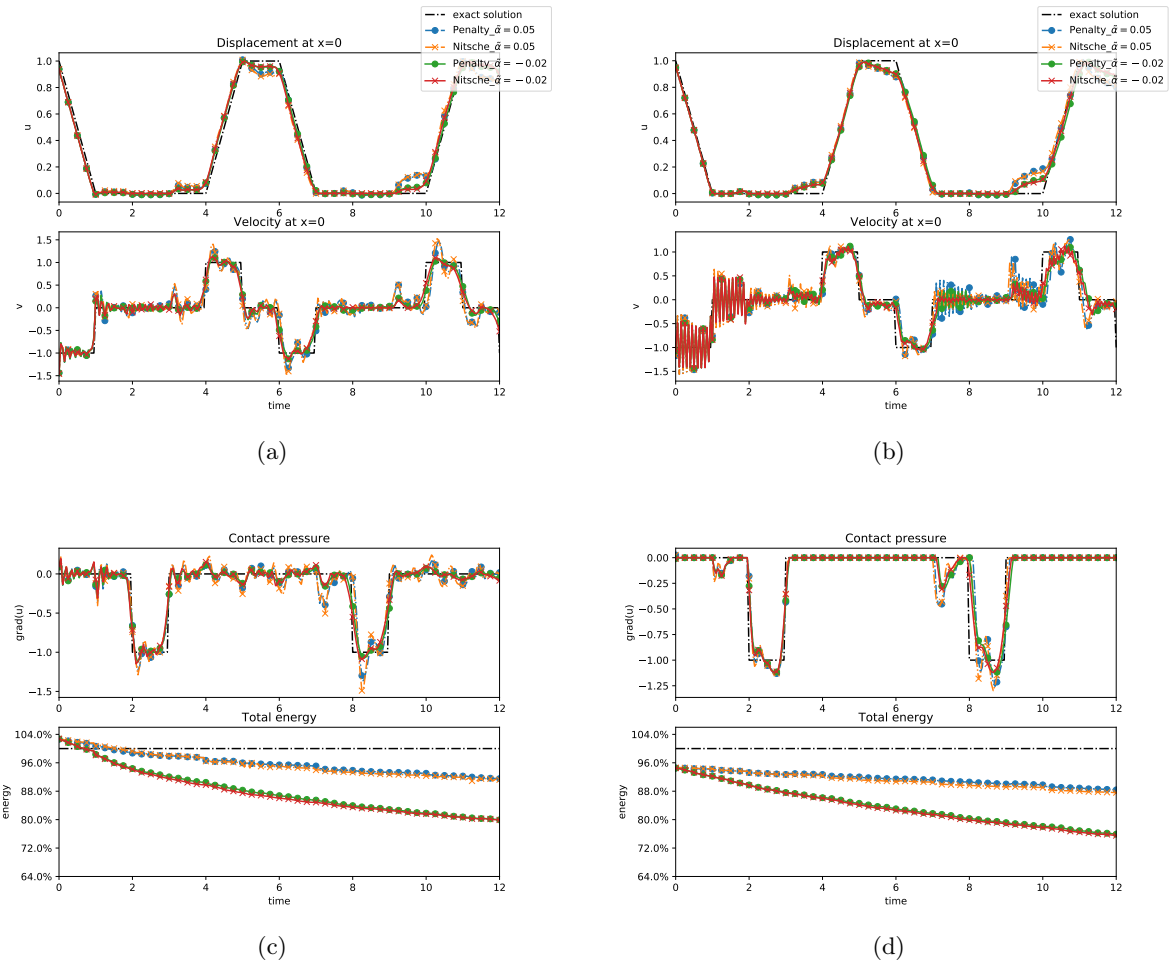

Figure 13: 1D-SS: Comparison of the analytical and discrete solutions for standard (left) and modified (right) mass matrices with HHT-α method and $\tilde{\alpha} \in \{0.05, -0.02\}$.

step is used. For a soft version, the Lamé coefficients are $\lambda = \mu = 20$, and $\Delta t = 0.25$; and for a hard version, the Lamé coefficients are $\lambda = \mu = 30000$, and $\Delta t = 0.05$. In both cases, the mass density $\rho = 1$, and the gravity load is $\mathbf{f} = [0, 0, -0.1]^T$. The lower part of the sphere is assigned with Signorini boundary conditions and on the upper part, a Neumann condition $\mathbf{f}_N = \mathbf{0}$ is applied. For the numerical simulation, quadratic Lagrange finite elements are used for the displacement and linear finite elements contact multiplier (when using the ALM). The Nitsche's parameter γ_0, the penalty parameter ϵ_0, and the parameter γ_a for ALM are chosen to be identical $\gamma_0 = \frac{1}{\epsilon_0} = \gamma_a = 100\mu$.

In Fig. 15 and Fig. 16, the results for soft and hard spheres are illustrated respectively for both Nitsche's method and ALM. Both schemes (the HHT-α scheme and the TRBDF2 scheme)

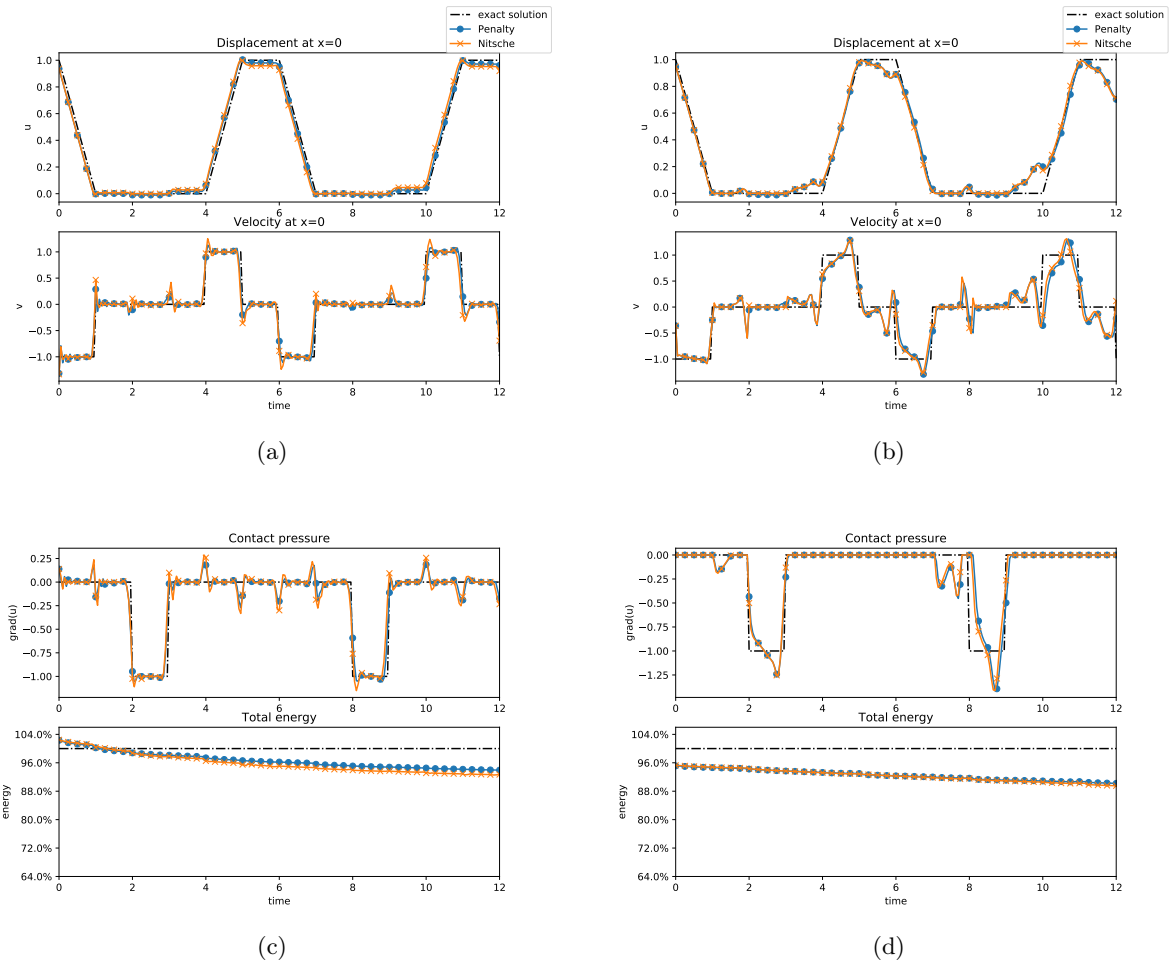

Figure 14: 1D-SS: Comparison of the analytical and discrete solutions for standard (left) and modified (right) mass matrices with TRBDF2 scheme.

produce a relatively smooth solution. As expected, the TR-BDF2 scheme provides smoother results for a comparable loss of energy than the HHT-α scheme. It is also noticed that the Nitsche hybrid scheme conserves very well the total modified energy as predicted by theory [20].

Acknowledgements

F.C.'s work is partially supported by the I-Site BFC project NAANoD and the EIPHI Graduate School (contract ANR-17-EURE-0002). F.C. is grateful for the Center for Mathematical Modeling grant FB20005.

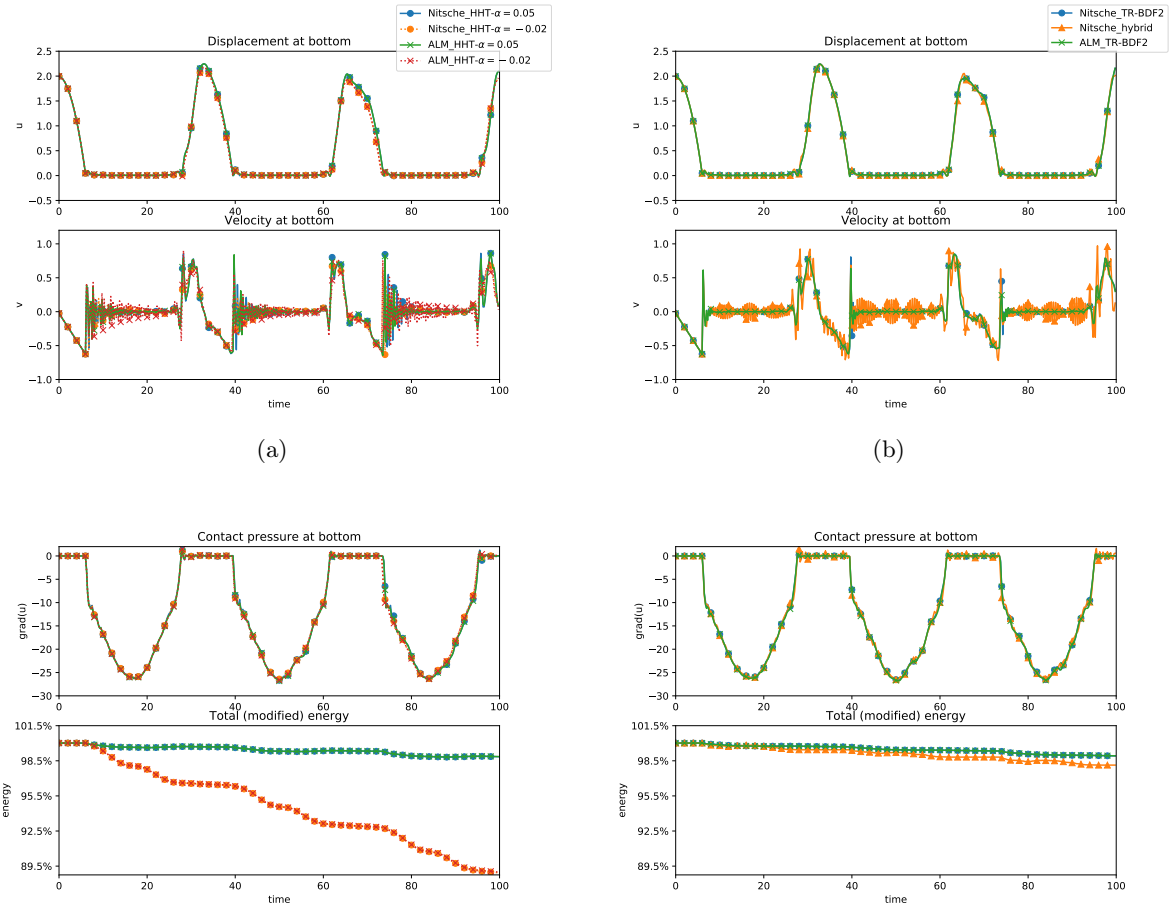

Figure 15: 3D impact of a soft sphere: Discrete solution for HHT-α (left), TR-BDF2 and Nitsche-hybrid (right) schemes.

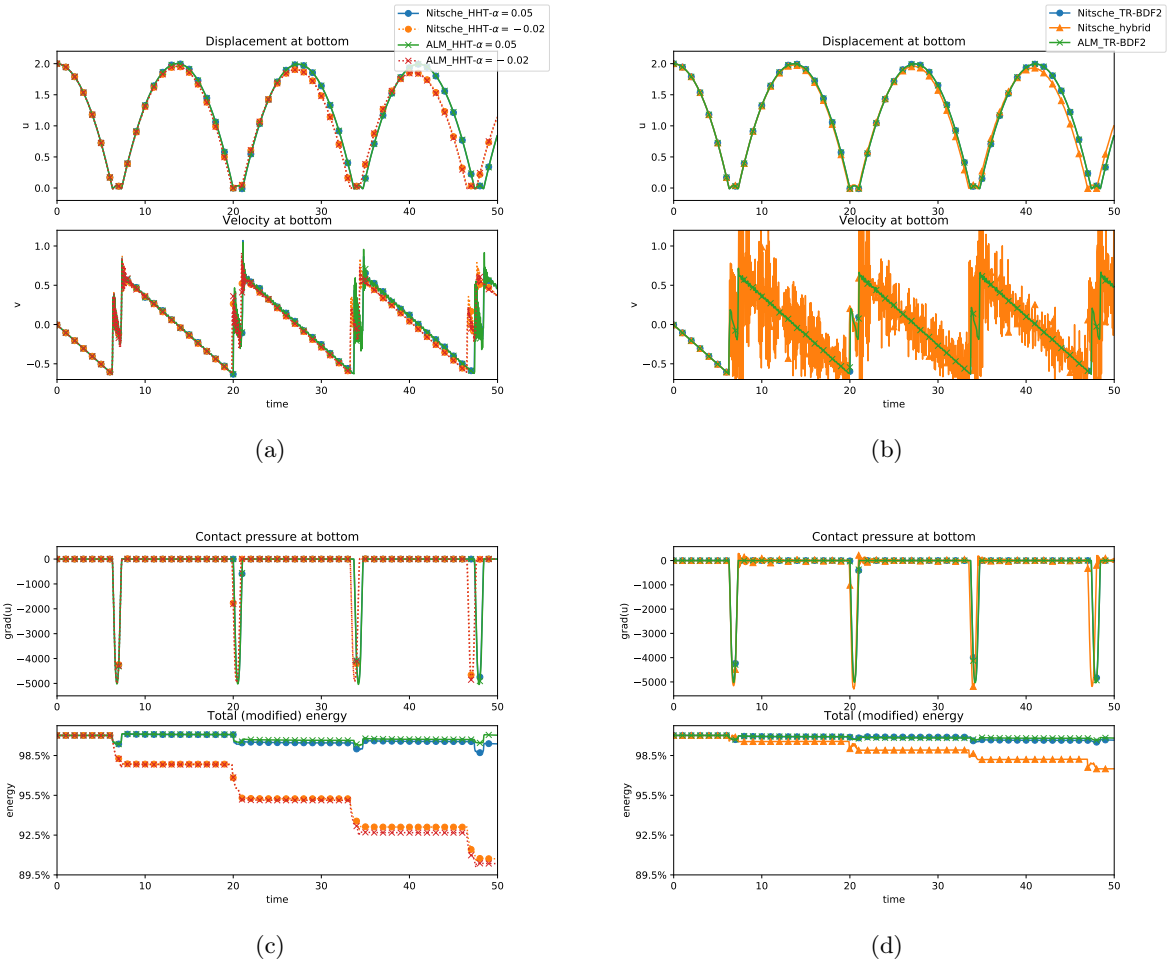

Figure 16: 3D impact of a hard sphere: Discrete solution for HHT-α (left), TR-BDF2 and Nitsche-hybrid (right) schemes.

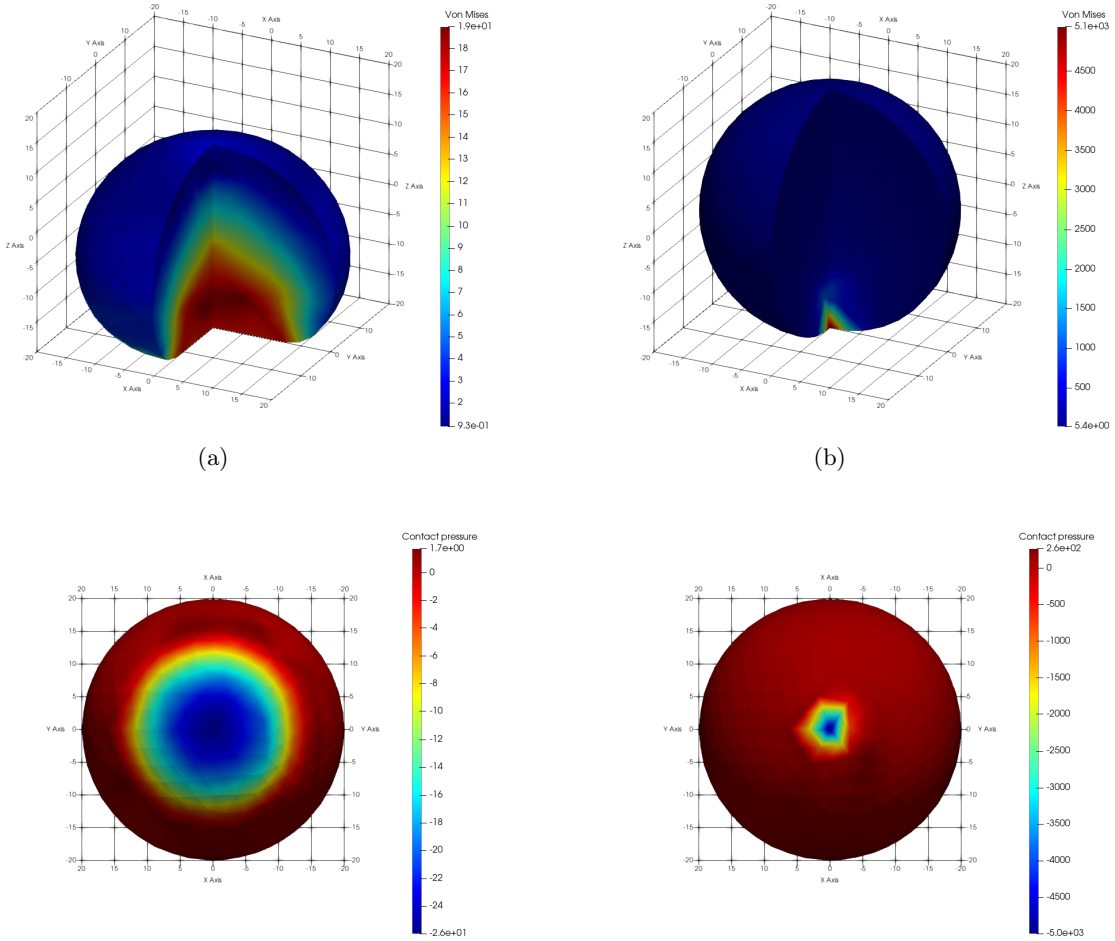

(a) (b)

(c) (d)

Figure 17: 3D impact of a soft sphere: deformed configuration with von Mises strain, and contact pressure for the soft sphere at $t = 16$ (left) and the hard sphere at $t = 6.8$ (right), for Nitsche's method with HHT-α scheme ($\tilde{\alpha} = 0.05$).

A Appendices

The first appendix details the local truncation error for the HHT-alpha scheme. The second appendix provides the complete amplification matrix for HHT-alpha.

A.1 Local truncation error for HHT-α scheme

Applying the local truncation error (27) to the SDOF system (25), the following holds:

$$
\begin{aligned}
\Delta t T_n =& \frac{-\tilde{\alpha}\omega^2\Delta t^2 + \frac{1}{\tilde{\beta}}}{\omega^2\Delta t^2\left(1-\tilde{\alpha}\right)+\frac{1}{\tilde{\beta}}}u(t^n) + \frac{\frac{1}{\tilde{\beta}}}{\omega^2\Delta t^2\left(1-\tilde{\alpha}\right)+\frac{1}{\tilde{\beta}}}\Delta t\dot{u}(t^n) \\
&+ \frac{1-2\tilde{\beta}}{2\tilde{\beta}\left(\omega^2\Delta t^2\left(1-\tilde{\alpha}\right)+\frac{1}{\tilde{\beta}}\right)}\Delta t^2\ddot{u}(t^n) - u(t^n) - \Delta t\dot{u}(t^n) - \frac{1}{2}\Delta t^2\ddot{u}(t^n) + O(\Delta t^3) \\
=& \frac{-\omega^2\Delta t^2}{\omega^2\Delta t^2\left(1-\tilde{\alpha}\right)+\frac{1}{\tilde{\beta}}}u(t^n) + \frac{\left(1-\tilde{\alpha}\right)\omega^2\Delta t^2}{\omega^2\Delta t^2\left(1-\tilde{\alpha}\right)+\frac{1}{\tilde{\beta}}}\Delta t\dot{u}(t^n) \\
&+ \frac{1}{2}\left(\frac{(1-2\tilde{\beta})\frac{1}{\tilde{\beta}}}{\omega^2\Delta t^2\left(1-\tilde{\alpha}\right)+\frac{1}{\tilde{\beta}}} - 1\right)\Delta t^2\ddot{u}(t^n) + O(\Delta t^3), \\
=& \frac{1}{\omega^2\Delta t^2\left(1-\tilde{\alpha}\right)+\frac{1}{\tilde{\beta}}}\left(-\omega^2\Delta t^2 u(t^n) - \left(1+\frac{\omega^2\Delta t^2\left(1-\tilde{\alpha}\right)}{2}\right)\Delta t^2\ddot{u}(t^n)\right) \\
&+ \frac{\left(1-\tilde{\alpha}\right)\omega^2\Delta t^2}{\omega^2\Delta t^2\left(1-\tilde{\alpha}\right)+\frac{1}{\tilde{\beta}}}\Delta t\dot{u}(t^n) + O(\Delta t^3) \\
=& \frac{1}{\omega^2\Delta t^2\left(1-\tilde{\alpha}\right)+\frac{1}{\tilde{\beta}}}\left(-\left(\omega^2 u(t^n) + \ddot{u}(t^n)\right)\Delta t^2 - \frac{\omega^2\Delta t^2\left(1-\tilde{\alpha}\right)}{2}\Delta t^4\ddot{u}(t^n)\right) \\
&+ \frac{\left(1-\tilde{\alpha}\right)\omega^2}{\omega^2\Delta t^2\left(1-\tilde{\alpha}\right)+\frac{1}{\tilde{\beta}}}\Delta t^3\dot{u}(t^n) + O(\Delta t^3) \\
\leq& \frac{1}{\omega^2\Delta t^2\left(1-\tilde{\alpha}\right)+\frac{1}{\tilde{\beta}}}\left|\omega^2 u(t^n) + \ddot{u}(t^n)\right|\Delta t^2 + \frac{\left(1-\tilde{\alpha}\right)\omega^2}{\omega^2\Delta t^2\left(1-\tilde{\alpha}\right)+\frac{1}{\tilde{\beta}}}\left|\dot{u}(t^n)\right|\Delta t^3 + O(\Delta t^3),
\end{aligned}
\tag{36}
$$

which implies the boundness of the local truncation error.

A.2 Amplification matrix for HHT-α scheme

The amplification matrix for the HHT-α scheme reads below:

$$\begin{bmatrix} \frac{-\tilde{\alpha}\tilde{\omega}^2+\frac{1}{\tilde{\beta}}}{\tilde{\omega}^2(1-\tilde{\alpha})+\frac{1}{\tilde{\beta}}} & \frac{1}{\tilde{\beta}\left(\tilde{\omega}^2(1-\tilde{\alpha})+\frac{1}{\tilde{\beta}}\right)} & \frac{1-2\tilde{\beta}}{2\tilde{\beta}\left(\tilde{\omega}^2(1-\tilde{\alpha})+\frac{1}{\tilde{\beta}}\right)} \\ \tilde{\gamma}\left(\frac{-\tilde{\alpha}\tilde{\omega}^2+\frac{1}{\tilde{\beta}}}{\tilde{\beta}\left(\tilde{\omega}^2(1-\tilde{\alpha})+\frac{1}{\tilde{\beta}}\right)}-\frac{1}{\tilde{\beta}}\right) & \tilde{\gamma}\left(-\frac{1}{\tilde{\beta}}+\frac{1}{\tilde{\beta}^2\left(\tilde{\omega}^2(1-\tilde{\alpha})+\frac{1}{\tilde{\beta}}\right)}\right)+1 & \tilde{\gamma}\left(\frac{2\tilde{\beta}-1}{2\tilde{\beta}}+\frac{1-2\tilde{\beta}}{2\tilde{\beta}^2\left(\tilde{\omega}^2(1-\tilde{\alpha})+\frac{1}{\tilde{\beta}}\right)}\right)-\tilde{\gamma}+1 \\ \frac{-\tilde{\alpha}\tilde{\omega}^2+\frac{1}{\tilde{\beta}}}{\tilde{\beta}\left(\tilde{\omega}^2(1-\tilde{\alpha})+\frac{1}{\tilde{\beta}}\right)}-\frac{1}{\tilde{\beta}} & -\frac{1}{\tilde{\beta}}+\frac{1}{\tilde{\beta}^2\left(\tilde{\omega}^2(1-\tilde{\alpha})+\frac{1}{\tilde{\beta}}\right)} & \frac{2\tilde{\beta}-1}{2\tilde{\beta}}+\frac{1-2\tilde{\beta}}{2\tilde{\beta}^2\left(\tilde{\omega}^2(1-\tilde{\alpha})+\frac{1}{\tilde{\beta}}\right)} \end{bmatrix}. \tag{37}$$

References

[1] P. Alart and A. Curnier. A mixed formulation for frictional contact problems prone to Newton like solution methods. *Computer methods in applied mechanics and engineering*, 92(3):353–375, 1991.

[2] F. Armero and E. Petőcz. Formulation and analysis of conserving algorithms for frictionless dynamic contact/impact problems. *Computer methods in applied mechanics and engineering*, 158(3-4):269–300, 1998.

[3] R. E. Bank, W. M. Coughran, W. Fichtner, E. H. Grosse, D. J. Rose, and R. K. Smith. Transient simulation of silicon devices and circuits. *IEEE Transactions on Computer-Aided Design of Integrated Circuits and Systems*, 4(4):436–451, 1985.

[4] K.-J. Bathe and M. M. I. Baig. On a composite implicit time integration procedure for nonlinear dynamics. *Computers & Structures*, 83(31-32):2513–2524, 2005.

[5] K. J. Bathe and E. L. Wilson. NONSAP — A nonlinear structural analysis program. *Nuclear Engineering and Design*, 29(2):266–293, 1974. Special Issue: Papers Presented at the Conference.

[6] É. Bretin and Y. Renard. Stable IMEX schemes for a Nitsche-based approximation of elastodynamic contact problems. Selective mass scaling interpretation. *The SMAI journal of computational mathematics*, 6:159–185, 2020.

[7] H. Brezis. Equations et inéquations non linéaires dans les espaces vectoriels en dualité. In *Annales de l'institut Fourier*, volume 18, pages 115–175, 1968.

[8] E. Burman, P. Hansbo, and M. G. Larson. Augmented Lagrangian finite element methods for contact problems. *ESAIM: Mathematical Modelling and Numerical Analysis*, 53(1):173–195, 2019.

[9] E. Burman, P. Hansbo, and M. G. Larson. The augmented Lagrangian method as a framework for stabilised methods in computational mechanics. *Archives of Computational Methods in Engineering*, pages 1–26, 2023.

[10] P. Cantin and P. Hild. Error analysis of the compliance model for the Signorini problem. *Calcolo*, 58(3):32, 2021.

[11] F. Chouly. An adaptation of Nitsche's method to the Tresca friction problem. *Journal of Mathematical Analysis and Applications*, 411(1):329–339, 2014.

[12] F. Chouly, A. Ern, and N. Pignet. A hybrid high-order discretization combined with Nitsche's method for contact and Tresca friction in small strain elasticity. *SIAM Journal on Scientific Computing*, 42(4):A2300–A2324, 2020.

[13] F. Chouly, M. Fabre, P. Hild, R. Mlika, J. Pousin, and Y. Renard. An overview of recent results on Nitsche's method for contact problems. *Geometrically unfitted finite element methods and applications*, pages 93–141, 2017.

[14] F. Chouly, M. Fabre, P. Hild, J. Pousin, and Y. Renard. Residual-based a posteriori error estimation for contact problems approximated by Nitsche's method. *IMA Journal of Numerical Analysis*, 38(2):921–954, 2018.

[15] F. Chouly and P. Hild. A Nitsche-based method for unilateral contact problems: numerical analysis. *SIAM Journal on Numerical Analysis*, 51(2):1295–1307, 2013.

[16] F. Chouly and P. Hild. On convergence of the penalty method for unilateral contact problems. *Applied Numerical Mathematics*, 65:27–40, 2013.

[17] F. Chouly, P. Hild, V. Lleras, and Y. Renard. Nitsche-based finite element method for contact with Coulomb friction. In *European Conference on Numerical Mathematics and Advanced Applications*, pages 839–847. Springer, 2017.

[18] F. Chouly, P. Hild, V. Lleras, and Y. Renard. Nitsche method for contact with Coulomb friction: existence results for the static and dynamic finite element formulations. *Journal of Computational and Applied Mathematics*, 416:114557, 2022.

[19] F. Chouly, P. Hild, and Y. Renard. A Nitsche finite element method for dynamic contact: 1. Space semi-discretization and time-marching schemes. *ESAIM: Mathematical Modelling and Numerical Analysis*, 49(2):481–502, 2015.

[20] F. Chouly, P. Hild, and Y. Renard. A Nitsche finite element method for dynamic contact: 2. Stability of the schemes and numerical experiments. *ESAIM: Mathematical Modelling and Numerical Analysis*, 49(2):503–528, 2015.

[21] F. Chouly, P. Hild, and Y. Renard. Symmetric and non-symmetric variants of Nitsche's method for contact problems in elasticity: theory and numerical experiments. *Mathematics of Computation*, 84(293):1089–1112, 2015.

[22] F. Chouly, R. Mlika, and Y. Renard. An unbiased Nitsche's approximation of the frictional contact between two elastic structures. *Numerische Mathematik*, 139(3):593–631, 2018.

[23] F. Chouly and Y. Renard. Explicit Verlet time-integration for a Nitsche-based approximation of elastodynamic contact problems. *Advanced Modeling and Simulation in Engineering Sciences*, 5(1):1–38, 2018.

[24] J. Chung and G. M. Hulbert. A Time Integration Algorithm for Structural Dynamics With Improved Numerical Dissipation: The Generalized-α Method. *Journal of Applied Mechanics*, 60(2):371–375, 06 1993.

[25] F. Dabaghi, A. Petrov, J. Pousin, and Y. Renard. A robust finite element redistribution approach for elastodynamic contact problems. *Applied Numerical Mathematics*, 103:48–71, 2016.

[26] N. Dirani and L. Monasse. An explicit pseudo-energy conservative scheme for contact between deformable solids. working paper or preprint, Nov. 2022.

[27] D. Doyen, A. Ern, and S. Piperno. Time-integration schemes for the finite element dynamic Signorini problem. *SIAM Journal on Scientific Computing*, 33(1):223–249, 2011.

[28] S. Erlicher, L. Bonaventura, and O. S. Bursi. The analysis of the generalized-α method for non-linear dynamic problems. *Computational mechanics*, 28(2):83–104, 2002.

[29] M. Fortin and R. Glowinski. *Augmented Lagrangian methods: applications to the numerical solution of boundary-value problems*. Elsevier, 2000.

[30] R. Glowinski and P. Le Tallec. *Augmented Lagrangian and operator-splitting methods in nonlinear mechanics*. SIAM, 1989.

[31] T. Gustafsson, R. Stenberg, and J. Videman. On Nitsche's method for elastic contact problems. *SIAM Journal on Scientific Computing*, 42(2):B425–B446, 2020.

[32] P. Hauret and P. Le Tallec. Energy-controlling time integration methods for nonlinear elastodynamics and low-velocity impact. *Computer Methods in Applied Mechanics and Engineering*, 195(37-40):4890–4916, 2006.

[33] M. R. Hestenes. Multiplier and gradient methods. *Journal of Optimization Theory and Applications*, 4(5):303–320, 1969.

[34] H. M. Hilber, T. J. Hughes, and R. L. Taylor. Improved numerical dissipation for time integration algorithms in structural dynamics. *Earthquake Engineering & Structural Dynamics*, 5(3):283–292, 1977.

[35] M. Hosea and L. Shampine. Analysis and implementation of TR-BDF2. *Applied Numerical Mathematics*, 20(1-2):21–37, 1996.

[36] T. J. Hughes. *The finite element method: linear static and dynamic finite element analysis*. Courier Corporation, 2012.

[37] M. Jalali Mashayekhi and J. Kövecses. A comparative study between the augmented Lagrangian method and the complementarity approach for modeling the contact problem. *Multibody System Dynamics*, 40(4):327–345, 2017.

[38] Y. Kanto and G. Yagawa. A dynamic contact buckling analysis by the penalty finite element method. *International Journal for Numerical Methods in Engineering*, 29(4):755–774, 1990.

[39] H. B. Khenous, P. Laborde, and Y. Renard. Mass redistribution method for finite element contact problems in elastodynamics. *European Journal of Mechanics-A/Solids*, 27(5):918–932, 2008.

[40] N. Kikuchi and J. T. Oden. *Contact problems in elasticity: a study of variational inequalities and finite element methods*. SIAM, 1988.

[41] A. Klarbring, A. Mikelić, and M. Shillor. Frictional contact problems with normal compliance. *International Journal of Engineering Science*, 26(8):811–832, 1988.

[42] R. Krause and M. Walloth. Presentation and comparison of selected algorithms for dynamic contact based on the Newmark scheme. *Applied Numerical Mathematics*, 62(10):1393–1410, 2012.

[43] T. Laursen and V. Chawla. Design of energy conserving algorithms for frictionless dynamic contact problems. *International Journal for Numerical Methods in Engineering*, 40(5):863–886, 1997.

[44] R. Mlika, Y. Renard, and F. Chouly. An unbiased Nitsche's formulation of large deformation frictional contact and self-contact. *Computer Methods in Applied Mechanics and Engineering*, 325:265–288, 2017.

[45] N. M. Newmark. A method of computation for structural dynamics. *Journal of the engineering mechanics division*, 85(3):67–94, 1959.

[46] J. Nitsche. Über ein variationsprinzip zur lösung von dirichlet-problemen bei verwendung von teilräumen, die keinen randbedingungen unterworfen sind. In *Abhandlungen aus dem mathematischen Seminar der Universität Hamburg*, volume 36, pages 9–15. Springer, 1971.

[47] G. Noh and K.-J. Bathe. For direct time integrations: A comparison of the Newmark and ρ_∞-Bathe schemes. *Computers & Structures*, 225:106079, 2019.

[48] J. Oden. Exterior penalty methods for contact problems in elasticity. *Nonlinear finite element analysis in structural mechanics*, pages 655–665, 1981.

[49] J. Oden and N. Kikuchi. Finite element methods for constrained problems in elasticity. *International Journal for Numerical Methods in Engineering*, 18(5):701–725, 1982.

[50] J. Oden and J. Martins. Models and computational methods for dynamic friction phenomena. *Computer Methods in Applied Mechanics and Engineering*, 52(1):527–634, 1985.

[51] L. Paoli and M. Schatzman. A numerical scheme for impact problems. I. The one-dimensional case. *SIAM J. Numer. Anal.*, 40(2):702–733, 2002.

[52] L. Paoli and M. Schatzman. A numerical scheme for impact problems. II. The multidimensional case. *SIAM J. Numer. Anal.*, 40(2):734–768, 2002.

[53] M. Powell. On nonlinear optimization since 1959. In *The Birth of Numerical Analysis*, pages 141–160. World Scientific, 2010.

[54] M. J. Powell. A method for nonlinear constraints in minimization problems. *Optimization*, pages 283–298, 1969.

[55] Y. Renard. Generalized Newton's methods for the approximation and resolution of frictional contact problems in elasticity. *Computer Methods in Applied Mechanics and Engineering*, 256:38–55, 2013.

[56] Y. Renard and K. Poulios. GetFEM: Automated FE modeling of multiphysics problems based on a generic weak form language. *ACM Transactions on Mathematical Software (TOMS)*, 47(1):1–31, 2020.

[57] R. D. Richtmyer and K. W. Morton. Difference methods for initial-value problems. *Malabar*, 1994.

[58] A. Seitz, W. A. Wall, and A. Popp. Nitsche's method for finite deformation thermomechanical contact problems. *Computational Mechanics*, 63:1091–1110, 2019.

[59] R. Stenberg. On some techniques for approximating boundary conditions in the finite element method. *Journal of Computational and Applied Mathematics*, 63(1-3):139–148, 1995.

[60] E. Süli and D. F. Mayers. *An introduction to numerical analysis*. Cambridge University Press, Cambridge, 2003.

[61] P. Wriggers and G. Zavarise. A formulation for frictionless contact problems using a weak form introduced by nitsche. *Computational Mechanics*, 41:407–420, 2008.